

HuD interacts with survival motor neuron protein and can rescue spinal muscular atrophy-like neuronal defects

Lisa Hubers[†], Hector Valderrama-Carvajal[†], Janik Laframboise, Janie Timbers, Gabriel Sanchez and Jocelyn Côté*

Department of Cellular and Molecular Medicine, Faculty of Medicine, University of Ottawa, Ottawa, Ontario, Canada K1H 8M5

Received August 29, 2010; Revised and Accepted November 15, 2010

Spinal muscular atrophy is an autosomal-recessive neuromuscular disease caused by disruption of the survival of motor neuron (SMN) gene, which promotes cytoplasmic assembly of the splicing core machinery. It remains unclear how a deficiency in SMN results in a disorder leading to selective degeneration of lower motor neurons. We report here that SMN interacts with RNA-binding protein HuD in neurites of motor-neuron-derived MN-1 cells. This interaction is mediated through the Tudor domain of SMN and, importantly, naturally occurring Tudor mutations found in patients with severe spinal muscular atrophy (SMA) completely abrogate the interaction, underscoring its relevance to the disease process. We also characterized a regulatory pathway involving coactivator-associated arginine methyltransferase 1 (CARM1) and HuD. Specifically, we show that CARM1 expression is rapidly downregulated, at the protein level, following induction of differentiation through retinoid and neurotrophic signaling. Using purified proteins, we demonstrate that methylation of HuD by CARM1 reduces its interaction with the *p21^{cip1/waf1}* mRNA, showing that CARM1 can directly influence RNA-binding activity. We further demonstrate that this CARM1-dependent regulatory switch mainly controls the activity of HuD in promoting cell-cycle exit, whereas the interaction between HuD and SMN is required for proper recruitment of HuD and its mRNA targets in neuronal RNA granules. Finally, we were able to rescue SMA-like defects in a hypomorphic *Smn* knockdown MN-1 cell line through overexpression of HuD. Together, these findings extend our understanding of specific role(s) of SMN in motor neurons and provide crucial insights into potential new avenues for SMA therapeutic strategies.

INTRODUCTION

Spinal muscular atrophy (SMA) is an autosomal-recessive neuromuscular disease and is distinguished by the selective degeneration of lower motor neurons of the spinal cord. SMA, with an incidence of approximately 1 in 6000 live births, is the most common genetic cause of infant mortality, where the more severe forms of the disease result in death before 2 years of age (1). Pathophysiology of SMA includes progressive weakness and wasting of the proximal voluntary muscles of the limbs, ultimately leading to paralysis, which eventually affects the entire trunk during disease progression (2). There are five clinical types of SMA, categorized

mainly by motor capabilities and age of onset, with Type 0 and Type I (Werdnig–Hoffman syndrome) being the most severe forms (3).

The causative gene for SMA is named as the ‘survival of motor neuron’ (*SMN*) gene (4). SMA is caused by deletions or loss-of-function mutations in the *SMN1* gene, leading to insufficient expression of the functional full-length SMN protein. SMN exists in most cells as a large macromolecular complex containing oligomerized SMN protein as well as seven Gemins and unrip (5–8). In the cytoplasm, this ‘core SMN complex’ functions in the assembly of Sm proteins and U small nuclear RNAs into small nuclear ribonucleoprotein particles (snRNPs) (9–11). Despite our detailed

*To whom correspondence should be addressed. Tel: +1 6135625800 ext. 8660; Fax: +1 6135625636; Email: jcote@uottawa.ca

[†]Authors contributed equally to this work.

knowledge of functions of SMN in the snRNP assembly process, the largely motor neuron-specific defect caused by a deficiency in this protein remains unexplained. Reduced snRNP assembly rates and decreased levels of specific snRNPs have been documented in fibroblasts from SMA patients and in various SMA-like conditions (12–14). Furthermore, various degrees of aberrant splicing profiles have been observed in animal models of SMA (13,15–17). However, it remains unclear whether a causal link exists between SMA motor neuron pathogenesis and defects in snRNP biogenesis (18–20).

Alternatively, more direct functions for SMN in axons (21–30), as well as in maturation of the neuromuscular junction (31–36), have been proposed. In neuronal processes, SMN still partially colocalizes with Gemins (37,38), as well as the RNA-binding protein heterogeneous nuclear RNP (hnRNP) R and β -actin mRNA (21,39), but not Sm proteins (27,37). Accordingly, mislocalization of β -actin mRNA and protein in both axons and growth cones has been observed in SMN-deficient motor neurons (21). Previously, we demonstrated that another RNA-binding protein, KSRP, interacts with SMN in neurites of differentiated neuronal cells (29). Importantly, KSRP protein was downregulated in SMA mice spinal cords, which correlated with an increase in p21^{cip1/waf1} mRNA, a target of KSRP (29).

Arginine methylation has been implicated in numerous cellular processes, including transcription, DNA repair, RNA processing, signal transduction and protein localization (reviewed in 40). The two major forms of methylated arginines found in eukaryotes are ω - N^G,N^G -asymmetric dimethylarginines (aDMA) and ω - N^G,N^G -symmetric dimethylarginines (sDMA). This methylation is accomplished by a family of enzymes termed the protein arginine methyltransferases (PRMTs) (41). Presently, nine PRMTs have been identified in mammals. All PRMTs can catalyze the formation of ω - N^G -monomethylated arginine (MMA), but Type I (PRMT1, 2, 3, 4, 6 and 8) and Type II (PRMT5) enzymes are distinguished by their ability to produce either aDMA or sDMA, respectively (40,42). The type of methylation reaction catalyzed by PRMT7 is still debated (43,44), and PRMT9 (4q31) has not been characterized biochemically to date. Both PRMT5 and PRMT7 methylate RG-rich sequences in the C-terminal domain of snRNP proteins SmD1, SmD3 and SmB/B', which provide a driving force for the snRNP assembly process by potentiating their transfer to the SMN complex (45–49). This methyl-sensing capacity of the SMN complex is conferred by the Tudor domain of SMN, which is a conserved protein–protein interaction module that specifically recognizes methylated arginine domains in other proteins (49–51). It was further uncovered that arginine methylation of p80 Coilin, the marker of Cajal bodies, promotes its interaction with SMN and likely mediates the recruitment of assembled snRNPs to these nuclear structures upon their nuclear import (52,53). More recently, it was found that PRMT4/coactivator-associated arginine methyltransferase 1 (CARM1) can also modulate the interactions of the SMN Tudor domain with its binding partners (29,54). Finally, naturally occurring SMN Tudor mutations that abolish interactions with several methylated cellular proteins are found in patients with severe Type I SMA, highlighting the clinical relevance of this conserved domain to the etiology

of the disease (49). Taken together, these observations indicate an important role for arginine methylation in the regulation of SMN activities.

Arginine methylation has been shown to regulate the differentiation of a number of cell lineages, including adipocytes, skeletal muscles and neuronal cells (55–60). However, mechanistic details as well as specific PRMT substrates remain largely unknown in most of these studies. In one particular study, it was shown that CARM1 participates in nerve growth factor (NGF)-induced differentiation of rat PC12 cells through methylation of the neuronal RNA-binding protein, HuD (61). More specifically, reducing CARM1 levels through RNA interference resulted in increased p21 mRNA (a known mRNA target of HuD) through extension of its half-life, thus mimicking the effect observed following NGF treatment. Further experiments showed that overexpression of an HuD mutant that cannot be methylated (R236K) also resulted in increased p21 levels. Using immunoprecipitation/reverse transcription–polymerase chain reaction (IP/RT–PCR) experiments, they provided evidence that more p21 mRNAs are associated with the HuD mRNP in cells transfected with the R236K mutant, suggesting that arginine methylation of HuD by CARM1 may regulate its interaction with target mRNAs. Finally, using pan methyl-dependent antibodies, it was shown that the pool of methylated HuD is reduced in NGF-treated PC12 cells, which led them to propose that following neurotrophic stimulation, HuD may either get directly demethylated or CARM1 activity may somehow be downregulated.

Hu proteins are the mammalian homologs of *Drosophila* embryonic lethal abnormal vision (ELAV) and they are a family of RNA-binding proteins implicated in almost all aspects of post-transcriptional regulation (reviewed in 62). HuD, along with HuC and HuB, constitutes the neuronal-specific family members, whereas the fourth mammalian homolog, HuR, is ubiquitously expressed (62). The neuronal Hu proteins are regulatory proteins required for the differentiation, maintenance and plasticity of neurons (reviewed in 63). HuD expression is first detectable in neurogenic precursors at the point of withdrawal from the mitotic cycle, and expression persists in mature neurons, consistent with a role early in neuronal specification and differentiation (reviewed in 64). Hu proteins interact with AU-rich RNA elements (AREs) in the 3'-untranslated regions (UTRs) of specific target mRNAs (reviewed in 62). Unlike many other ARE-binding proteins that predominantly destabilize transcripts, Hu proteins prevent degradation of their target mRNAs, significantly prolonging their half-life and allowing increased protein production (65–69). HuD interacts with numerous, developmentally regulated transcripts including c-fos, c-myc and p21 (70–73). Consistent with its function in neuronal differentiation, many of the transcripts stabilized by HuD are involved in the formation of neuronal processes, including growth-associated protein 43 (GAP43), tau and acetylcholinesterase (65–67,69,74).

We report here that HuD and SMN interact in neurites of differentiated motoneuron-derived MN-1 cells. This interaction is mediated through the Tudor domain of SMN, and naturally occurring Tudor mutations found in patients with severe SMA abolished the interaction, underscoring its likely

implication in the disease process. In determining the functional relevance of the HuD/SMN interaction, we confirmed the existence and further characterized, in motoneuron-derived cells, a regulatory pathway involving CARM1 and HuD initially identified in PC12 cells (61). Specifically, we show that CARM1 expression is rapidly downregulated, at the protein level, following induction of differentiation through retinoic acid and neurotrophic signaling. Using biochemical and quantitative approaches, we demonstrate that methylation of HuD by CARM1 reduces its interaction with p21 mRNA 3'UTR sequences. Although this CARM1-dependent regulatory switch mainly affected cell-cycle exit, the interaction between HuD and SMN was required for proper recruitment of HuD and its mRNA targets into neuritic RNA granules. Finally, we were able to rescue SMA-like defects in a hypomorphic SMN knockdown MN-1 motor neuron cell line through overexpression of HuD. Together, these findings extend our understanding of SMN-specific role(s) in motor neurons and provide crucial insights into potential new avenues for SMA therapeutic strategies.

RESULTS

HuD interacts with the Tudor domain of SMN in MN-1 cells

Based on our recent findings that RNA-binding protein KSRP interacted with SMN in neuronal processes (29), we wanted to determine whether HuD may also behave similarly and exist in a complex with SMN. HuD is an RNA-binding protein that is known to promote differentiation and functional maintenance of many types of neurons, including motor neurons (63,64,75), so it constituted a good candidate to potentially uncover novel function(s) for SMN in this cell type. In order to assess the potential interaction between SMN and HuD, endogenous HuD was immunoprecipitated from MN-1 cell extracts, and the retained proteins were resolved by sodium dodecyl sulfate–polyacrylamide gel electrophoresis (SDS–PAGE) and analyzed by western blotting for the presence of HuD (Fig. 1A, lanes 1–3) and then SMN (lanes 4–6). Endogenous SMN was detected in the HuD immunoprecipitate, but not in control IgG IPs (Fig. 1A, lanes 6 and 5, respectively). As both SMN and HuD are known components of RNP complexes, we next wanted to assess whether the co-IP we observed was dependent on the presence of RNA. To do so, the co-IPs were carried out from MN-1 cell extracts that had been either pre-incubated in the presence of RNase A or mock-treated (29), and the presence of SMN was assessed by immunoblotting. Under both conditions, an equivalent amount of SMN was detected in the HuD immunoprecipitate (data not shown), indicating that the interaction is likely not mediated via an RNA moiety.

The exon 3-encoded Tudor domain in SMN constitutes its major protein–protein interaction surface (see 49 and references therein), so we next wanted to determine whether this domain was responsible for mediating the HuD interaction. Total cell extracts from MN-1 cells were subjected to GST-pull-down experiments using either GST alone or a GST fusion with the Tudor domain of SMN (Fig. 1B; GST-Tdr). HuD bound to the GST-Tdr column, but not to

GST alone, suggesting that the interaction could be mediated through the SMN Tudor domain (Fig. 1B, middle panel, lanes 3 and 2, respectively). Intriguingly, the amount of HuD protein detected with the Tudor domain was greatly reduced in the presence of RNase A in comparison to Mock-treated extracts (Fig. 1B, lanes 4–6). The fact that the co-IP between SMN and HuD was, in contrast, resistant to RNase treatment may suggest that these two proteins interact in a larger complex in cells, which prevents accessibility to nucleases and may stabilize the interaction. Importantly, binding was abolished (Fig. 1C) by intragenic Tudor mutations found in human patients with severe Type I SMA (2,76,77). Furthermore, the SMA-causing E134K mutation also abolished the interaction between SMN and HuD when introduced in the context of the full-length SMN protein (Fig. 1D), suggesting that the Tudor domain is both sufficient and required for HuD binding. In order to determine whether these proteins interact directly, a blot overlay approach (Far-Western) was used (Fig. 1E). Endogenous HuD was immunoprecipitated from MN-1 cell lysates, and proteins were resolved by SDS–PAGE and transferred to a nitrocellulose membrane at low voltage. Purified GST-Tdr was then used to probe the membrane, followed by extensive washing and standard anti-GST immunoblotting. We have previously used this approach to demonstrate that the Tudor domain of SMN interacted with a number of cellular proteins from HeLa cell extracts (49), and a similar pattern was observed in MN-1 total cell lysates (Fig. 1E, lanes 1 and 3). Strikingly, a band was also observed in the HuD immunoprecipitate (Fig. 1E, lane 4), and the identity of that band was further confirmed by reblotting the membrane using anti-HuD (Fig. 1E, lane 6). As the signal observed was relatively weak, we next performed the same experiment with more starting material and also included a specificity control where the HuD antibody was omitted. With this increased molar ratio, a clear signal was now observed in the HuD immunoprecipitate but not in the mock IP (Fig. 1E; right panel, lanes 2 and 1, respectively), strongly suggesting that HuD can bind directly the Tudor domain of SMN. Taken together, these results show that SMN and HuD interact in MN-1 cells, and this interaction is likely mediated through the SMN Tudor domain.

SMN and HuD interact in neurites of differentiated MN-1 cells

We next wanted to assess whether HuD and SMN colocalized in MN-1 cells. The intracellular localization of SMN and HuD in fixed cells is well established (69,78–82). SMN localizes mostly in the cytoplasm and concentrates in bright nuclear foci corresponding to Gems and/or Cajal bodies, as seen in undifferentiated MN-1 cells (Fig. 2A, SMN panel). In contrast, HuD is diffusely distributed throughout the cytoplasm at steady state (Fig. 2A, HuD panel). Hence, apart from the obvious overlap in the cytoplasmic diffuse staining, no additional colocalization was observed between the two proteins in undifferentiated MN-1 cells (Fig. 2A, merge panel). Indirect immunofluorescence microscopy for SMN and HuD was then performed on MN-1 cells induced to differentiate through the addition of *trans*-retinol and GDNF for 48 h. Both HuD and SMN were found in granular foci along neuritic

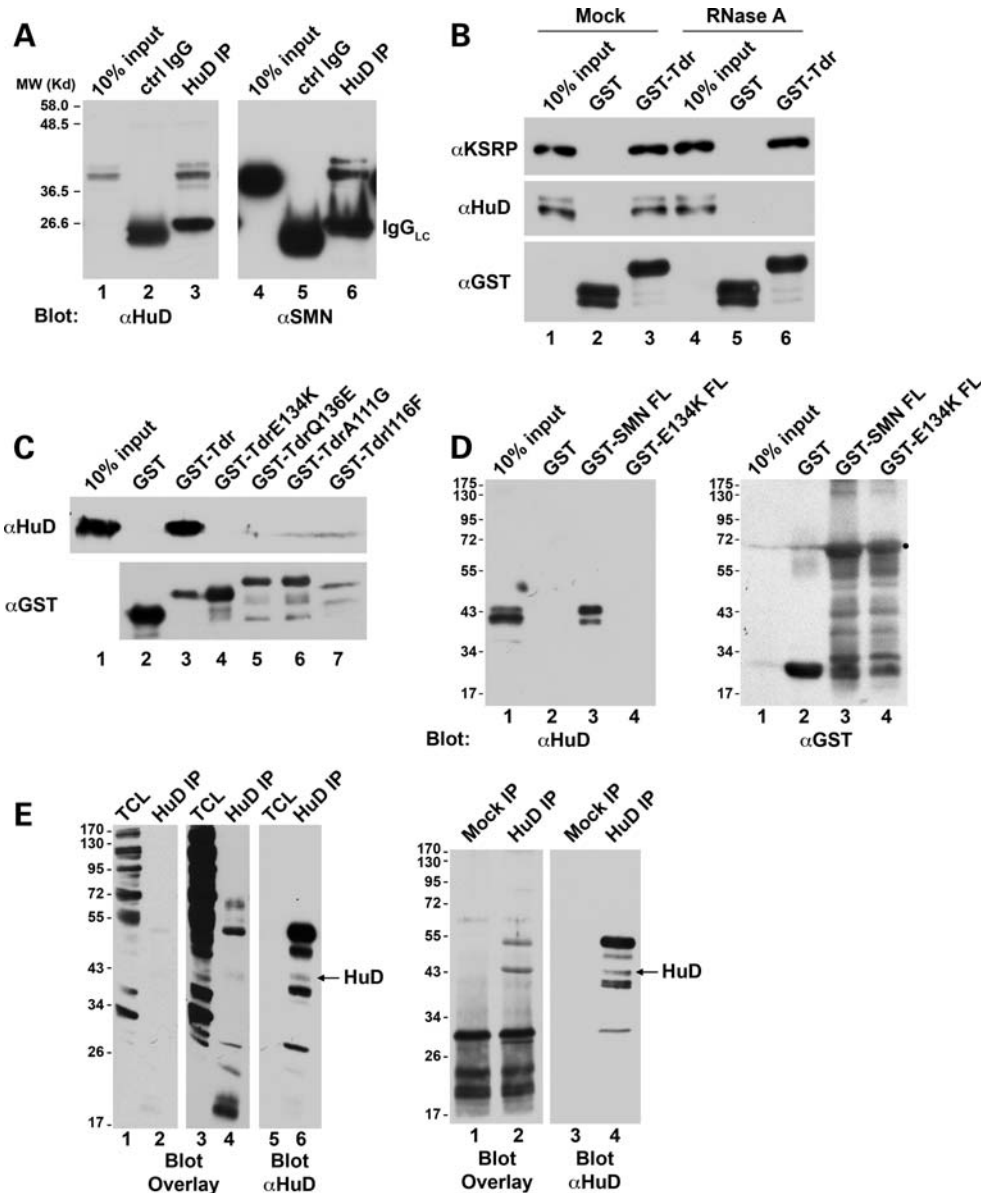


Figure 1. HuD interacts with the Tudor domain of SMN in MN-1 cells. Endogenous HuD was immunoprecipitated (IP) from MN-1 cells and the resulting immunoprecipitated proteins were analyzed by western blot using antibodies against HuD (left panel) and SMN (right panel). Migration of the antibodies' immunoglobulin heavy chain (IgG) is indicated (A). Total cell lysates were prepared from MN-1 cells and subjected to binding assays using immobilized GST or SMN Tudor domain (GST-Tdr). Retained proteins were then immunoblotted for the presence of HuD. The same experiment was performed with or without pretreatment of the cell lysate with RNase A, indicating that the interaction between HuD and SMN Tudor domain is RNA dependent. The same membrane was stripped and reprobed for the presence of KSRP. Abundance of GST-fusion proteins was assessed using anti-GST immunoblotting (B). SMA-causing mutant alleles of the Tudor domain (GST-TdrE134K, GST-TdrQ136E, GST-TdrI116F and GST-TdrA111G) abolish binding of HuD (C). GST-pull-down assays show that the E134K mutation also abrogates HuD binding in the context of the full-length SMN protein (D). A blot overlay approach confirms that the SMN Tudor domain can interact directly with HuD. Endogenous HuD was immunoprecipitated from MN-1 cell lysates, resolved by SDS-PAGE and transferred to nitrocellulose membranes. Membranes were then incubated with purified GST-SMN-Tudor and retained protein following extensive washes were detected by anti-GST immunoblotting. Shorter (left panels, lanes 1 and 2) and longer (left panels, lanes 3 and 4) exposures of the anti-GST blot overlay are shown. HuD immunoblotting was then performed on that same membrane to identify the position of HuD (left panels, lanes 5 and 6). The same experiment was repeated with an increased ratio of starting lysates (right panels). Again a direct interaction was detected with a slower-migrating form of HuD (indicated by an arrow) in the HuD immunoprecipitate and not in a mock IP in which antibodies were omitted (right panels, compare lane 2 with 1, respectively) (E).

extensions (Fig. 2B). Interestingly, in neurites, $36.4 \pm 9.5\%$ of HuD foci also contained SMN, and $48.9 \pm 15\%$ of SMN foci contained HuD (Fig. 2B, bar graph). In order to confirm and also determine where in the cell the HuD and SMN physical interaction existed, we used the bimolecular fluorescence complementation (BiFC) approach (83). This assay has been

used extensively to detect non-covalent interactions between proteins of many different structural classes in virtually every subcellular compartment (84 and references therein). For this, cDNAs encoding HuD or SMN (wild-type and E134K mutant alleles) were subcloned to create a fusion with either the N-terminal fragment of yellow fluorescent

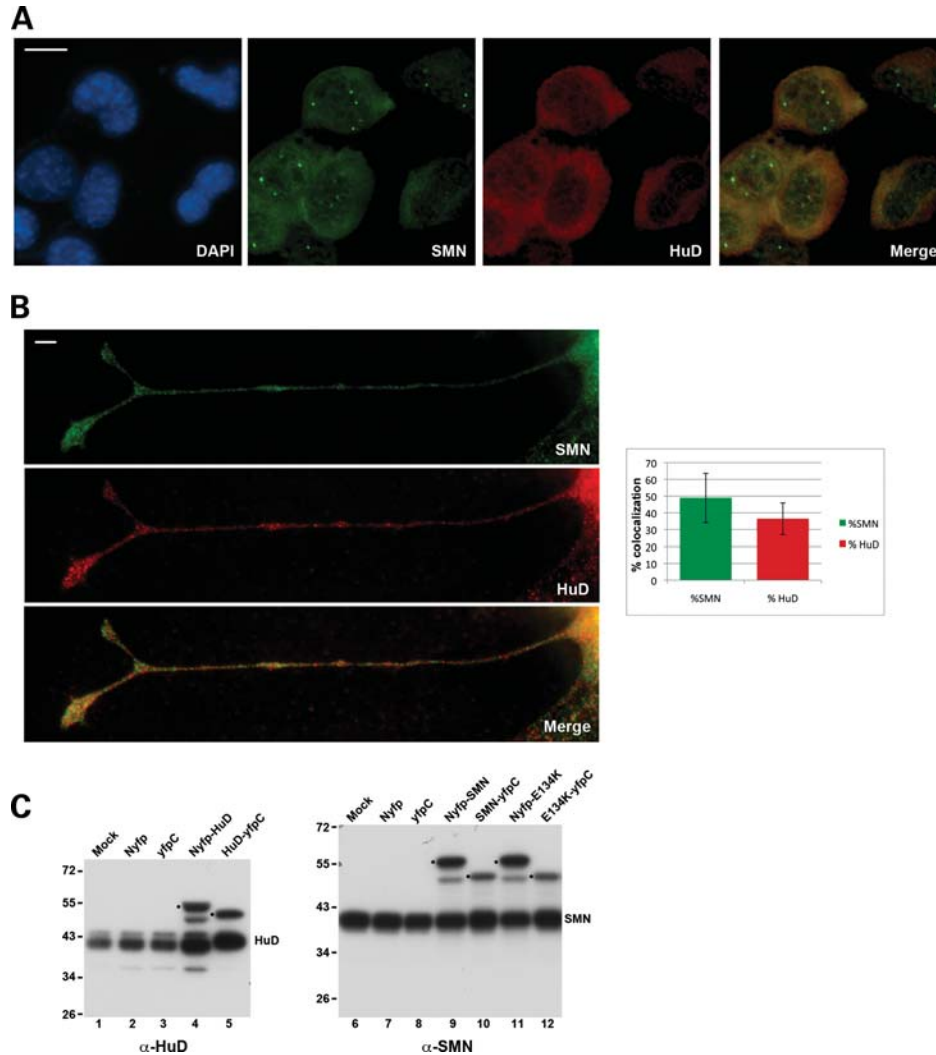


Figure 2. SMN and HuD physically interact in neurites of differentiated MN-1 cells. Undifferentiated MN-1 cells were labeled for immunofluorescence with HuD or SMN antibodies. Merged images reveal no colocalization between HuD and SMN apart from the diffuse cytoplasmic staining. Bar, 20 μ m (A). Images captured at 63 \times and focusing on neurites of differentiated MN-1 cells reveal the presence of both SMN (top) and HuD (middle) in bright granular foci along extending neurites. Foci where both proteins colocalized quantified as followed: $36.4 \pm 9.5\%$ of HuD-positive foci also contained SMN, and $48.9 \pm 15\%$ of SMN-positive foci contained HuD (bar graph shows the mean % of signal colocalized \pm SEM; $n = 20$ neurites). Bar, 20 μ m (B). Proper expression of the various fusion protein constructs used in BiFC experiments was confirmed by immunoblotting with anti-HuD or anti-SMN antibodies, as indicated. Migration of endogenous HuD and SMN is indicated on the right of each panel, and fusion proteins are labeled with a ‘•’ (C). BiFC was used to confirm physical interaction between HuD and SMN in cells. As a validation for the approach, N- and C-terminal YFP fragment fusion constructs of either HuD or SMN were transfected in undifferentiated MN-1 cells and shown to reconstitute YFP fluorescence in patterns identical to the respective intracellular distribution of endogenous proteins (Nyfp-HuD/HuD-yfpC: panels a–c; and Nyfp-SMN/SMN-yfpC: panels d–f). When SMN and HuD YFP fragment fusions are combined, reconstitution of the YFP signal can be seen predominantly in the cytoplasm (Nyfp-HuD/SMN-yfpC: panels m–o) as an indication that they can physically interact in cells. As an internal control for the assay, the E134K mutant allele does not promote reconstitution of the YFP fluorescence when combined with HuD (Nyfp-HuD/E134K-yfpC: panels p–r), although they can promote interaction in the context of mutant homodimers (Nyfp-E134K/E134K-yfpC: panels j–l) or heterodimers with the wild-type SMN protein (Nyfp-E134K/SMN-yfpC: panels g–i) (D). Two representative examples are shown where SMN and HuD BiFC fusions are seen to physically interact in bright foci along neuronal processes (panels a–c and d–f). Bars, 20 μ m (E). Cell nuclei were counter-stained with DAPI.

protein (YFP; Nyfp-HuD/SMN) or the C-terminal fragment of YFP (HuD/SMN-yfpC). Proper expression of each fusion protein was confirmed by immunoblotting (Fig. 2C). As both SMN and HuD are known to oligomerize (85,86), N- and C-ter YFP fragment fusion constructs of either HuD or SMN were first co-transfected in undifferentiated MN-1 cells in order to validate the system. Combining HuD with HuD resulted in a diffuse cytoplasmic fluorescent signal similar to the distribution obtained for endogenous HuD (Fig. 2D,

panels a–c), whereas transfection of either Nyfp-HuD or HuD-yfpC alone did not yield any detectable fluorescence (Supplementary Material, Fig. S1). Similarly, combining SMN YFP fusion constructs resulted in a typical endogenous SMN intracellular distribution (Fig. 2D, panels d–f), whereas again, transfection of either fusion constructs alone did not yield any detectable fluorescence (Supplementary Material, Fig. S1). Together, these controls show that the BiFC approach can be used to detect protein–protein

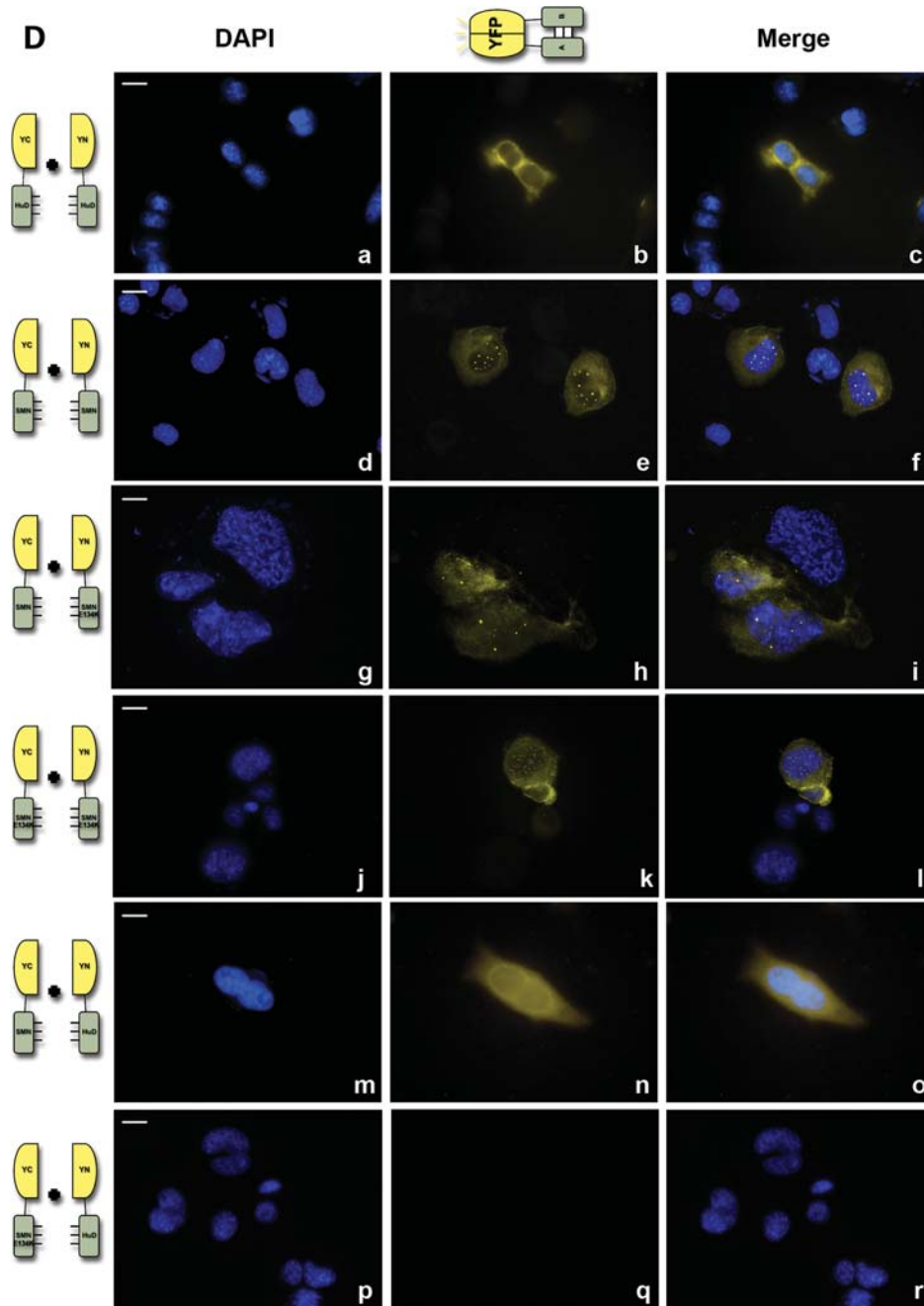


Figure 2. Continued

interactions in cells, and most importantly reveal where in the cell these interactions are taking place. Next, the Nyfp-HuD and SMN-yfpC constructs were co-transfected in undifferentiated MN-1, and 24–48 h post-transfection cells were fixed and visualized under a fluorescence microscope. As predicted from our biochemical experiments, SMN and HuD interacted with each other in cells, resulting in a reconstituted YFP signal with a mostly diffuse cytoplasmic distribution (Fig. 2D, panels m–o). All cells positive for an YFP signal showed similar distribution, suggesting that the HuD/SMN interaction occurs predominantly in the cytoplasm and not in nuclear Gems/

Cajal bodies. As an internal control for this assay, SMN fusion constructs harboring the E134K Tudor domain mutation were also engineered (Fig. 2C). This mutation does not prevent the SMN protein from localizing to the cytoplasm and Cajal bodies, although it often leads to accumulation of mutant proteins in an increased number of Gems (87,88). Consistent with this, combination of wild-type SMN and SMN-E134K yielded an YFP signal resembling normal endogenous SMN distribution (Fig. 2D, panels g–i), whereas mutant proteins together most often led to an increased number of nuclear foci (Fig. 2D, panels j–l). In

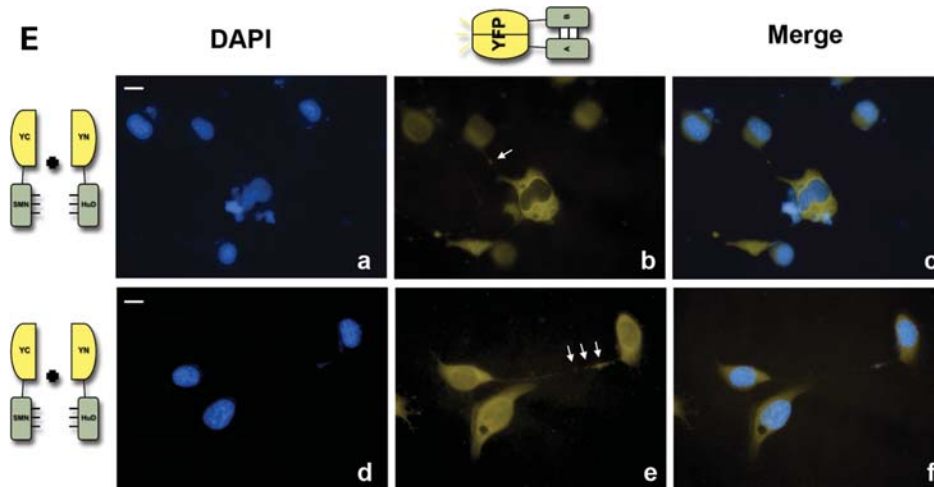


Figure 2. Continued

contrast, combining HuD and mutant SMN-E134K fusion proteins did not yield any detectable fluorescence (Fig. 2D, panels p–r). The same experiment was also performed with MN-1 cells induced to differentiate 18 h post-transfection and processed for fluorescence microscopy after 48 h in differentiation media (Fig. 2E). As seen in undifferentiated cells, all YFP-positive cells showed a diffuse cytoplasmic signal, although the YFP signal was also observed within discrete foci localized to neurites of differentiated cells (Fig. 2E, panels b and e). Taken together, these results confirm a direct interaction between SMN and HuD that mostly occurs in the cytoplasm and within neurites of differentiated motoneuron-like cells.

CARM1 is required to maintain motoneuron-derived MN-1 cells in a proliferative state

We have previously reported that a transient knockdown of CARM1 was sufficient to induce neurite outgrowth in MN-1 cells (29). As mentioned above, arginine methylation of HuD by CARM1 was shown to regulate the switch between proliferation and differentiation in PC12 cells (61). In order to characterize this regulatory pathway further in motor neurons, a stable derivative of the MN-1 cell line with reduced CARM1 expression was generated using an shRNA-expressing vector approach (Fig. 3A). As seen with a transient knockdown of CARM1, a significant increase in the number of cells with neuronal processes extending at least two times the length of the cell body was observed in the MN-1 CARM1 knockdown stable cell line (Fig. 3B). This effect on neurite extension was comparable to that obtained when MN-1 cells are induced to differentiate using a combination of 50 μ M *trans*-retinol and GDNF in media containing reduced serum levels (Fig. 3B, bar graph). In contrast, no effect on neurite extension was observed when a stable MN-1 cell line was derived using either the empty vector or the same vector expressing an shRNA targeting a different arginine methyltransferase, namely PRMT5 (Fig. 3B and data not shown, respectively). Accordingly, loss of CARM1

resulted in a small but significant ($P = 0.0267$) reduction in proliferation rate relative to the empty vector control, as determined by monitoring BrdU incorporation (Fig. 3C). This partial effect may be because of the selective pressure in generating a stable knockdown derivative as it is still possible to reduce the proliferation rate further through RA/GDNF-induced differentiation (Fig. 3C). In PC12 cells, it was found that cell-cycle exit following NGF treatment (or CARM1 knockdown) was mainly regulated through stabilization of HuD mRNA target, p21^{cip1/waf1} (61). In order to assess whether p21 was also the main CDK inhibitor targeted downstream of CARM1 in MN-1 cells, cell lysates from Mock and shCARM1 cells were immunoblotted for p21 (Fig. 3D, left panel). Consistent with the slight reduction in cell proliferation, a modest but significant increase in p21 was observed in stable CARM1 knockdown MN-1 cells when compared with empty vector control cells (Fig. 3D, left panel). Reverse transcription followed by quantitative PCR (RT-qPCR) was next used to monitor p21 mRNA levels in the CARM1 knockdown cell line derivative, and consistent with protein levels, a \sim 3-fold increase was observed for p21 mRNA (Fig. 3D, bar graph). This effect was enhanced further by reducing CARM1 expression to even lower levels (see western blot in Fig. 3A) using a transient siRNA knockdown strategy in the shCARM1 stable line (Fig. 3D, bar graph), establishing an inverse correlation between CARM1 expression and p21 mRNA level. Furthermore, the profile of p21 mRNA induction observed in the face of siRNA-reduced CARM1 expression closely mirrored that of RA/GDNF-induced differentiation (Fig. 3E), which points to CARM1 as a major player in the regulation of motor neuron differentiation.

In order to determine whether CARM1 overexpression was able to rescue the observed effects on differentiation, three different siRNAs, targeting sequences in the 3'UTR of endogenous *Carm1*, were procured (see Materials and Methods). Transfection of these siRNAs as a pool in MN-1 cells resulted in a significant decrease in *Carm1* mRNA and protein levels (Supplementary Material, Fig. S2). As was observed with our initial si/shRNA targeting sequence, this

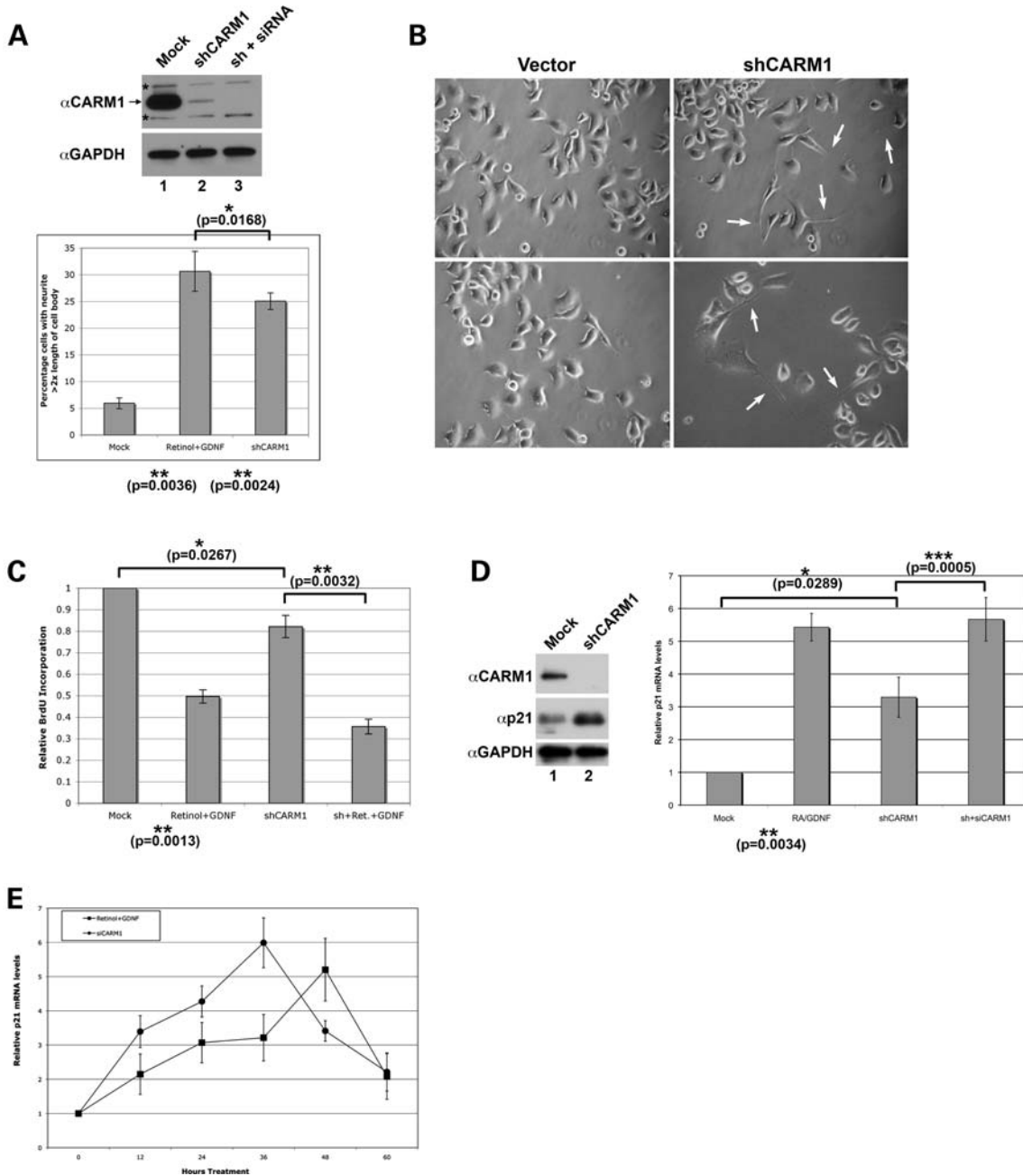


Figure 3. CARM1 is required to maintain motoneuron-derived MN-1 cells in a proliferative state. Stable knockdown of CARM1 in MN-1 cells using an shRNA-expressing vector was assessed by immunoblotting (lanes 1 and 2). Transient transfection of an siRNA in these stable knockdown cell lines results in further reduction in CARM1 protein levels (lane 3). Appearance of non-specific cross-reacting bands is indicated by ‘•’ on the immunoblot (A). CARM1 knockdown cells exhibit a differentiated phenotype in comparison to cells transfected with empty vector. Representative phase-contrast images are shown. Arrows indicate neurites (B). BrdU assays demonstrate that shCARM1 cells show a statistically significant reduction in proliferation, albeit less pronounced than cells treated with differentiation media. Knockdown cells in the presence of differentiation media produced a further decrease in proliferation. Bar graph shows relative BrdU incorporation \pm SD, normalized to the empty vector control ($n = 5$) (C). p21 mRNA levels are increased upon MN-1 differentiation and in CARM1 knockdown cells. Reducing expression further using transient siRNA transfection results in upregulation comparable to differentiation media. Bar graph shows relative p21 mRNA levels \pm SD, normalized to the empty vector control, as determined by RT-qPCR ($n = 5$). Stable reduction of CARM1 levels also results in an upregulation of p21 protein levels (left panel) (D). Time course of p21 mRNA induction following transient siRNA knockdown of CARM1 closely mirrors that observed upon RA/GDNF-induced differentiation. Graph shows relative p21 mRNA levels \pm SD, normalized to the empty vector control, as determined by RT-qPCR ($n = 5$) (E). Statistical significance is indicated above bar graphs.

reduction in CARM1 levels was associated with an induction of neuronal differentiation (Supplementary Material, Fig. S2C, Mock and siCARM1-3’UTR panels). Quantification of this effect confirmed an increase in the percentage of cells with

long neurites (Supplementary Material, Fig. S2D), as well as an upregulation of p21 mRNA levels (Supplementary Material, Fig. S2E), comparable to the effects observed with our initial ORF-targeting si/shRNAs (compare with Fig. 3).

As the neuronal differentiation induced by reducing CARM1 expression likely triggers a cascade of molecular events, we reasoned that it might be difficult to revert these effects by re-expressing CARM1 after the fact. Alternatively, exogenous CARM1 overexpression prior to siRNA treatment should be able to compensate for the reduction in endogenous CARM1 and prevent induction of a differentiation phenotype. To test this hypothesis, GFP-CARM1 was introduced in parental MN-1 cells, ~10 h before transfection of the 3'UTR-targeting pool of siRNAs, and cell cultures were then monitored for differentiation. As expected, GFP-CARM1 expression was resistant to treatment using the 3'UTR-targeting siRNAs, whereas, in contrast, it was efficiently targeted and downregulated by our initial ORF-targeting siRNA (Supplementary Material, Fig. S2B and data not shown). Strikingly, cell cultures pre-transfected with GFP-CARM1 continued to proliferate at 48 h after treatment with the 3'UTR-targeting siRNAs when compared with mock-transfected controls (Supplementary Material, Fig. S2C). Accordingly, induction of a differentiation phenotype was not as evident in GFP-CARM1-expressing cells (Supplementary Material, Fig. S2C). This tendency was also observed on the whole-cell population as induction of neurite outgrowth and p21 mRNA levels were reduced to ~50% of that observed with either the 3'UTR-targeting siRNAs alone or the combination of GFP-CARM1 and the ORF-targeting siRNA (Supplementary Material, Fig. S2, panels D and E). Taken together, our results demonstrate a direct correlation between CARM1 expression levels and maintenance of motoneuron-derived MN-1 cells in a non-differentiated state.

CARM1 is downregulated during MN-1 differentiation

In order to investigate this phenomenon further, we devised an assay to monitor for endogenous CARM1 activity during differentiation of MN-1 cells. First, a standard *in vitro* methylation assay was performed using bacterially produced GST-CARM1 and GST-HuD. As was previously reported (61), GST-HuD was strongly methylated by CARM1 in this assay, when compared with the known CARM1 substrate SmB (Fig. 4A, compare lanes 3 and 2, respectively). In contrast, HuD was not a substrate for GST-PRMT1, although the latter had strong activity towards its known substrate hnRNP A1 (Fig. 4A, lanes 6 and 5, respectively). Finally, neither enzymes showed any activity towards GST alone (Fig. 4A, lanes 1 and 4). Taken together, these results indicated that at least a certain degree of substrate specificity towards GST-HuD could be maintained *in vitro*. Thus, we reasoned that using cell extracts from MN-1 cells as a source of enzyme and GST-HuD as a substrate should provide us with a measure of endogenous CARM1 activity. MN-1 cellular extracts were prepared using a combination of sonication and detergent (see Materials and Methods for details) at different time points following RA/GDNF treatment and were used for *in vitro* methylation assays. Extracts prepared from undifferentiated MN-1 cells had comparable activity towards CARM1 substrates GST-SmB and GST-HuD (Fig. 4B, lanes 2 and 3, respectively), but not towards GST alone (Fig. 4B, lane 1). Strikingly, methylation activity towards GST-HuD was reduced ~50% after 12 h of

differentiation regimen and became barely detectable after 24 h of differentiation onwards (Fig. 4B, lanes 4–7). Importantly, no activity was detected towards GST-HuD when extracts were prepared from MN-1 cells transfected with an shRNA targeting CARM1 expression (Fig. 4B, lane 8), confirming that CARM1 is the only PRMT capable of methylating GST-HuD in these extracts.

To determine whether this downregulation of CARM1 activity correlated with protein levels, immunoblotting was performed on extracts from the differentiation time points used in the methylation assay. Western blotting clearly demonstrated that CARM1 protein levels were downregulated and became undetectable as early as 12 h following addition of differentiation media (Fig. 4C, top panel), whereas expression of SMN and HuD remained mostly constant (Fig. 4C, respective panels). Interestingly, *Carm1* downregulation was not observed at the mRNA level as determined using RT-qPCR (Fig. 4D), suggesting that CARM1 expression is regulated at the level of protein stability and/or translation during motoneuron differentiation. As an alternative indicator of CARM1 activity, the same extracts were immunoblotted with an antibody designed to recognize CARM1 methylation of Histone H3 arginine 17 (α H3R17me2a), but that was shown to cross-react with a number of other CARM1 substrates (54). In MN-1 cells, this antibody recognized approximately 10 proteins, most of which were no longer detected in extracts treated from CARM1 knockdown cells (Fig. 4C, lanes 1 and 6, respectively), strongly suggesting that these bands correspond to endogenous CARM1 substrates. Accordingly, a reduction in the immunoreactivity was seen, albeit to different extent, for most of these bands during MN-1 differentiation (Fig. 4C, lanes 1–5). Importantly, a band corresponding to HuD molecular weight showed a drastic reduction in α H3R17me2a immunoreactivity (indicated with an arrow in Fig. 4C), consistent with a decrease in HuD methylation level during MN-1 differentiation. Thus, activation of retinoic and neurotrophic signaling in MN-1 cells results in downregulation of CARM1 protein levels and HuD methylation, further indicating a key role for this methyltransferase in the maintenance of the proliferative state.

CARM1 methylation of HuD reduces its direct binding to p21 mRNA 3'UTR

It was previously reported that more p21 mRNA could be found co-purified with a non-methylatable HuD mutant IP when compared with transfected wild-type HA-tagged HuD (61). This result prompted the authors to suggest that CARM1 methylation may regulate HuD RNA-binding activity. In order to verify this directly, we prepared GST-HuD from bacteria and used it to perform RNA mobility shift assays with a radio-labeled p21 mRNA 3'UTR fragment harboring AU-rich elements previously shown to constitute binding sites for HuD (72). Unmethylated GST-HuD was able to bind p21 mRNA as a slower-migrating RNA species was detected in the presence of 10 ng of purified GST-HuD (Fig. 5A, lanes 1–3). In contrast, 100 ng of protein was required to observe a significant RNA shift when GST-HuD was pre-incubated with purified CARM1 under methylation conditions (Fig. 5A, lanes 4–6), suggesting that methylation

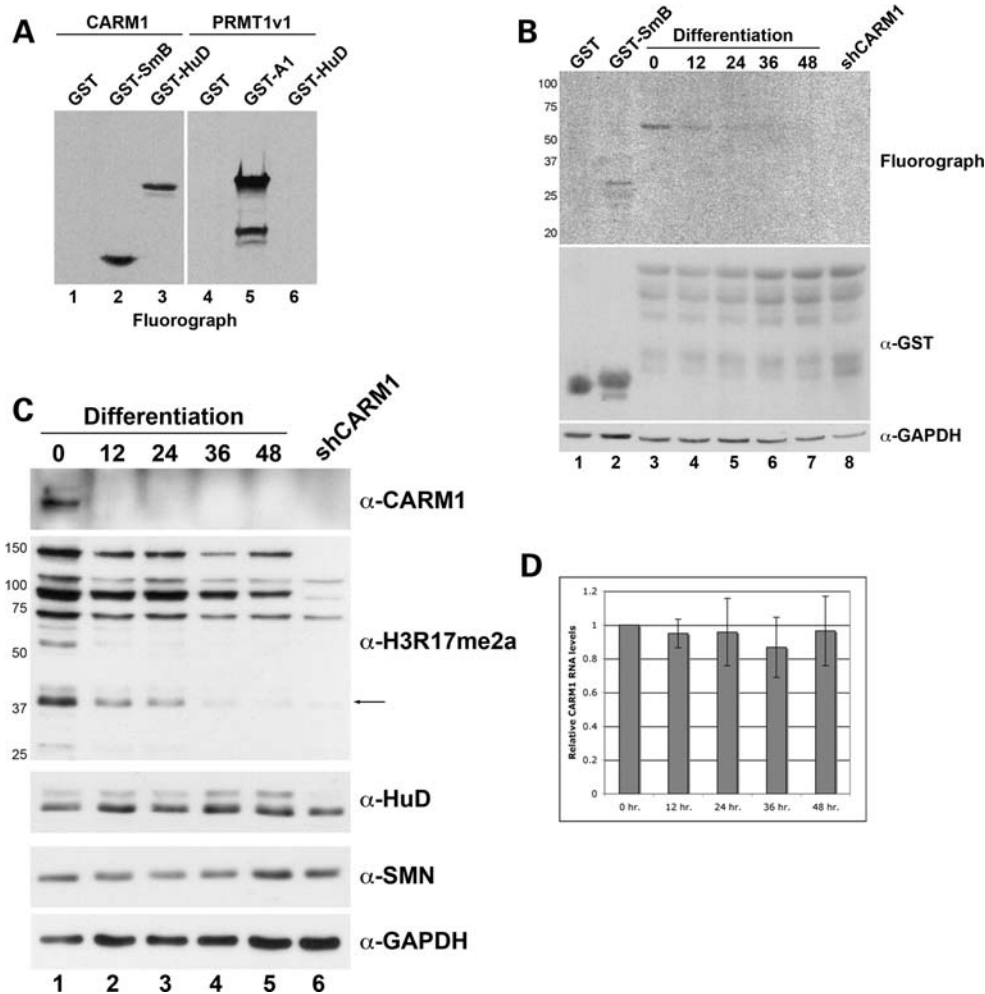


Figure 4. CARM1 is downregulated during MN-1 differentiation. *In vitro* methylation assays visualized through fluorography confirm that GST-HuD is a substrate for CARM1 and indicate that substrate specificity is conserved in these assays. GST-SmB is a positive control for CARM1 and GST-A1, for PRMT1v1 enzymes. GST alone is used as a negative control (A). *In vitro* methylation assays were performed using MN-1 cell extracts taken at the indicated time during differentiation as a source of enzyme. GST-HuD was used as a substrate. GST-SmB is used as a positive control and GST as a negative control. Extracts prepared from shCARM1 cells do not possess any methylase activity toward GST-HuD. Equal loading of GST-fusion substrates is assessed using anti-GST immunoblotting and equal amounts of methylating extracts are confirmed using anti-GAPDH (B). Western blot analysis of extracts prepared from MN-1 cells following the indicated time of differentiation. CARM1 protein level decreases within 12 h treatment. H3R17me2a, an antibody that specifically recognizes CARM1-methylated proteins, shows that the methylation status of numerous substrates is decreased in this process. One of the bands appears at a molecular weight corresponding to HuD, as indicated by an arrow. Immunoblotting for SMN and HuD indicates that the levels of these proteins do not change significantly during differentiation. GAPDH is used as a loading control (C). CARM1 mRNA levels remain constant in MN-1 differentiation, as determined using RT-qPCR. Bar graph shows relative CARM1 mRNA levels \pm SD, normalized to 0 h differentiation time point ($n = 4$) (D).

reduces HuD RNA-binding affinity for p21 mRNA 3'UTR. To make this assessment more quantitative, a filter-binding assay was used. Specifically, increasing amounts of unmethylated or CARM1-methylated GST-HuD were spotted on nitrocellulose filters in individual slots, and a fixed amount of radio-labeled p21 mRNA 3'UTR was allowed to flow through. Radioactivity retained in each slot was then quantified using a scintillation counter. The respective binding curves were plotted and used to calculate binding constants. Using this approach, it was determined that unmethylated HuD binds to the p21 mRNA 3'UTR sequence with a K_d of 24.37 μ M, whereas methylation of HuD resulted in a \sim 3-fold increase in apparent K_d (Fig. 5B). These results clearly demonstrate that CARM1 methylation significantly reduces the affinity of HuD for its mRNA target p21.

To determine whether this effect could be extended to other mRNA targets, we next immunoprecipitated endogenous HuD from either parental, empty vector control or CARM1 knock-down MN-1 cell lines and monitored for the presence of various known HuD mRNA targets using RT-PCR. In addition to p21 mRNA, *GAP43*, *Tau* and *Nova-1* mRNAs were amplified from the HuD immunoprecipitate, whereas GAPDH was not (Fig. 5C, lane 3, respective panels). As previously reported (61), a greater amount of p21 mRNA was immunoprecipitated with HuD from CARM1 knockdown MN-1 (Fig. 5C, lane 6, top panel, compare lane 9 with lanes 3 and 6). This enrichment in the face of reduced CARM1 expression was also observed for GAP43 mRNA, but not for Tau or Nova-1 (Fig. 5C, respective panels). The enrichment for p21 and GAP43 mRNA was also confirmed using RT-qPCR, with

normalization to the amount of HuD protein immunoprecipitated from each cell line extracts (Fig. 5D). Taken together, these results suggest that the influence of CARM1 methylation on HuD RNA-binding activity may be target-specific although this will require further investigation.

CARM1 methylation of HuD regulates its interaction with the SMN Tudor domain

We previously reported that CARM1 can regulate the interaction of some of its substrates with the Tudor domain of SMN (29,54). To determine whether methylation of HuD may also modulate its interaction with SMN, GST-pull-downs were performed as in Figure 1B, using either Mock (empty vector) or CARM1 knockdown MN-1 cell extracts as a source of proteins (Fig. 5E). The amount of endogenous HuD detected in pull-downs using the CARM1 knockdown cells was diminished relative to that from the mock extract (Fig. 5E, compare lane 6 with 3), indicating that CARM1 methylation of HuD can enhance its interaction with the SMN Tudor domain. Nevertheless, as was the case for RNase sensitivity, this effect of CARM1 was not observed in HuD/SMN co-IP experiments (data not shown).

Arginine methylation of R248 modulates HuD function in motoneuron differentiation

HuD overexpression was shown to be sufficient to induce neuronal differentiation in PC12 cells, cortical primary culture neurons and retinoic acid-induced embryonic stem (ES) cells (89,90). In order to further study the precise function and regulation of HuD in the differentiation of motoneuron-derived MN-1 cells, a plasmid encoding myc epitope-tagged HuD was generated and used for overexpression experiments. A representative example of the extent of overexpression obtained at 48 h post-transfection relative to endogenous HuD (~3-fold) is shown in Figure 6A. Under these conditions, ~30% of MN-1 cells extended long neurites upon myc-HuD overexpression, whereas no significant difference was observed between parental MN-1 (Mock) and transfection of the empty vector (Fig. 6D, myc-HuD, Mock and myc-pCDNA panels, respectively, and Fig. 6E). Accordingly, myc-HuD overexpression resulted in a 4-fold increase in p21 mRNA levels relative to the empty vector control, as determined by RT-qPCR (Fig. 6F). These effects are comparable to what is observed when MN-1 cells are induced to differentiate using *trans*-retinol and neurotrophic stimuli (e.g. see Fig. 3), suggesting that HuD is a central player downstream of these differentiation signals in motoneuron-derived MN-1 cells.

The increased ratio of HuD in comparison to constant CARM1 levels may result in a lower proportion of HuD being methylated, hence mimicking the situation observed during differentiation, which is consistent with the proposed model that an increased proportion of unmethylated HuD upregulates p21 and promotes neurite outgrowth. Thus, downstream of CARM1, it may be the relative amount of unmethylated to methylated HuD that regulates its function in MN-1 differentiation. The precise amino acid targeted by CARM1 for methylation has been mapped for HuR (91) and rat HuD (61), and corresponds to a highly conserved

arginine residue within the so-called 'hinge region' of ELAV family members (Fig. 6B; corresponds to R248 in mouse HuD). In order to test whether methylation of this residue can indeed regulate HuD activity in differentiating MN-1 cells, two amino acid substitutions were engineered at position 248 of myc-HuD (Fig. 6B; R248K and R248W). The R248K mutation renders this position non-methylatable by CARM1, while preserving the size and positive charge of arginine. In contrast, the R248W substitution should potentially create a 'methylmimetic', by introducing local hydrophobicity and bulkiness similar to the addition of two methyl groups (92). Transfections were performed as above, and equal expression of wild-type and mutant alleles of HuD was confirmed by immunoblotting after 48 h (Fig. 6C). Both wild-type and mutant HuD proteins were able to induce differentiation of MN-1 cultures, as monitored by phase-contrast microscopy and by calculating the percentage of cells extending long neurites (Fig. 6D and E). As would be predicted by the model proposed above, myc-HuD-R248K (which cannot be methylated by CARM1) was slightly more efficient at promoting neurite extension relative to wild-type or the R248W mutant (Fig. 6D and E). However, the R248W mutant allele, which should mimic a constitutively methylated HuD behaved essentially as wild type, as no statistically significant differences could be measured between myc-HuD and myc-HuD-R248W transfected cultures (Fig. 6E). A similar trend was observed for p21 mRNA level, with myc-HuD-R248K inducing a 5.5-fold increase in p21 mRNA levels relative to less than 4-fold for wild-type HuD (Fig. 6F). In contrast, however, no statistically significant effects on p21 levels relative to the empty vector control were observed following overexpression of the R248W mutant (Fig. 6F). Taken together, these results indicate that modification of R248 can indeed act as regulatory switch for HuD function in differentiation. Nevertheless, this residue would appear to be more critical in regulating the activity of HuD in its promotion of cell-cycle exit (i.e. upregulation of p21 levels) relative to neurite extension.

MN-1 cells with reduced SMN levels exhibit various differentiation defects

It has been reported in a number of neuronal cell lines, including PC12 (21,93) and N2a (29), as well as in primary motor neuron cultures (21), that reduced SMN levels cause various defects in neuritogenesis. Another study showed that neurospheres from SMA model mice generated neural stem cells that had an increased proliferation rate when induced to differentiate and that these cells had fewer and shorter neurites (94). As we have determined that SMN interacts with HuD, a protein known to regulate neuronal differentiation at many levels, including cell-cycle exit and neurite extension, we wanted to characterize further the effect(s) of reducing SMN levels in motoneuron-derived MN-1 cells. A stable knock-down of SMN was generated in MN-1 cells using an shRNA-expressing vector targeting a sequence in the 3'UTR of endogenous *Smn* (see Materials and Methods for details). Following selection, cells transfected with the SMN targeting shRNA showed ~50–60% reduction in SMN protein levels

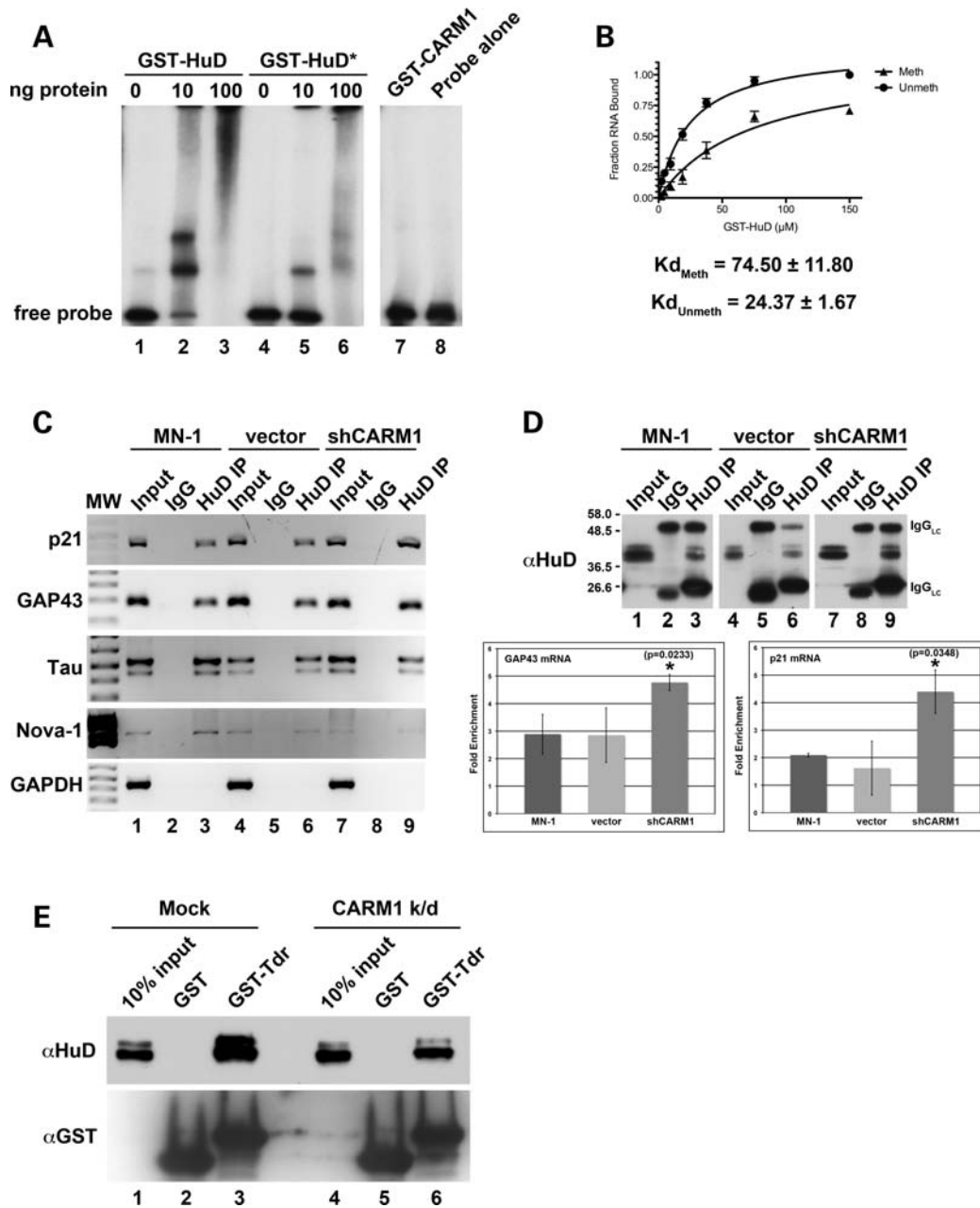


Figure 5. CARM1 methylation of HuD reduces its direct binding to p21 mRNA 3'UTR and modulates its interaction with SMN Tudor domain. RNA mobility shift assays monitoring the ability of methylated and unmethylated HuD to bind ³²P-p21 3'UTR RNA fragment. GST-HuD was subjected to *in vitro* methylation assays in the presence of GST-CARM1 (GST-HuD*) or GST (GST-HuD). The indicated amount of protein was then incubated with a constant amount of radio-labeled p21 RNA. GST-CARM1 alone does not bind the p21 RNA (A). Binding curves of both methylated and unmethylated HuD for p21 using nitrocellulose filter-binding assays (*n* = 3). Nonlinear regression analysis was used to calculate apparent *K_d* values (B). HuD was immunoprecipitated from extracts prepared from parental MN-1, empty vector control or shCARM1 cells, and RT-PCR was performed using primers specific for the indicated mRNAs. Increased amounts of p21 and GAP43 mRNAs, but not Tau and Nova-1 mRNAs, were detected in association with the HuD immunoprecipitate in shCARM1 cells. GAPDH is used as a negative control (C). These observations were confirmed using qPCR. RNAs used for qPCR reactions were normalized to the amount of HuD immunoprecipitated in each cell line as determined using immunoblotting (top panel). Bar graphs show average fold enrichment ± SD, over IgG control (*n* = 3). Statistical significance is indicated above bar graphs (D). CARM1 methylation enhances HuD binding to SMN Tudor domain. GST-pull-down assays were performed as in Figure 1 with GST-Tdr, using either empty vector control (Mock) or CARM1 knockdown cell lysates (CARM1 k/d) as source of proteins (E).

relative to MN-1 cultures transfected with the empty shRNA vector (Fig. 7A). When these cells were induced to differentiate using RA/GDNF treatment, the percentage of SMN knockdown cells that extended long neurites was reduced by almost 50% relative to control cells (Fig. 7A, bar graph and

Fig. 7B, representative phase-contrast images). This is consistent with the effect observed in the studies mentioned above using different neuronal cell lines. However, none of these studies assessed a potential impact of reduced SMN levels on cell-cycle exit, which may be expected because of its

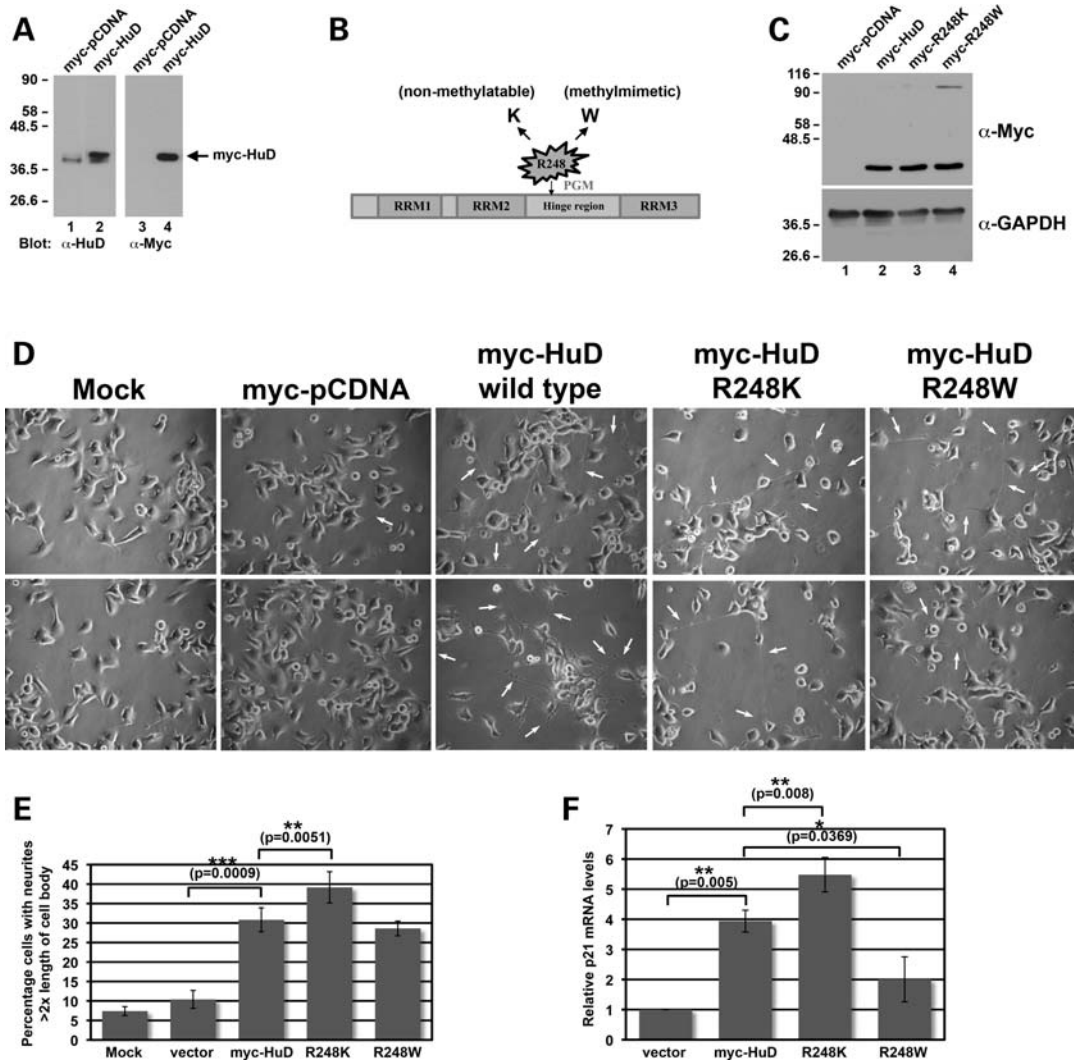


Figure 6. Arginine methylation of R248 modulates HuD function in motoneuron differentiation. Cell extracts from empty vector (myc-pCDNA) or myc-HuD transfections were used for immunoblotting with either anti-HuD (left panel) or anti-myc (right panel) antibodies. Migration of myc-HuD is indicated with an arrow. Transfection of myc-HuD in MN-1 cells results in a ~ 3 -fold overexpression relative to endogenous HuD levels (A). A schematic representation of the HuD protein is shown, indicating the position of R248 relative to conserved RNA Recognition Motifs (RRMs). Sequences flanking R248 are rich in PGM residues. R248 was mutagenized to either a lysine residue (K; non-methylatable) or a tryptophan (W; methylmimetic) (B). Representative immunoblot showing equal expression of myc-HuD alleles in MN-1 cells (C). Representative phase-contrast images showing induced neurite extension in cells transfected with myc-HuD alleles, relative to MN-1 cells incubated with transfection reagent alone (Mock) or empty vector control (myc-pCDNA) (D). Overexpression of HuD wild-type and mutant alleles induces neurite extension. Bar graph shows average percentage of cells with long neurites ($>2 \times$ length of cell body) \pm SD ($n = 4$) (E). Overexpression of HuD wild-type and R248K mutant results in p21 mRNA induction, whereas no effect is observed with HuD R248W. Bar graph shows relative p21 mRNA levels \pm SD, normalized to empty vector control, as determined by RT-qPCR ($n = 4$) (F). Statistical significance is indicated above respective bar graphs.

interaction with HuD. To address this, control and shSMN knockdown cultures were induced to differentiate, and their proliferation rate was measured using BrdU incorporation as a surrogate indicator. No difference in proliferation was observed in the shSMN cultures in the absence of differentiation stimuli (Fig. 7C). As expected, a reduction in BrdU incorporation was observed for control cells following RA/GDNF treatment (Fig. 7C, dark grey bars). A reduction in BrdU incorporation was also detected for shSMN knockdown cultures, although the extent of this reduction was reproducibly less than for control cells (Fig. 7C, light grey bars). Accordingly, a similar trend was seen with p21 mRNA levels, i.e. p21 mRNA induction following RA/GDNF

treatment was not as extensive in shSMN knockdown cultures relative to control cells (Fig. 7D), as determined using RT-qPCR. Taken together, these results suggest that, in addition to its previously reported role in neuritogenesis, SMN may also contribute to cell-cycle exit regulation in motor neurons, potentially through its interaction with HuD.

SMN is required for localization of HuD and its mRNA targets into RNA granules

HuD is found in the cytoplasm, but also in neuronal processes, where it resides in the so-called RNA granules with some of its mRNA targets (95–98). Thus, we next wanted to determine

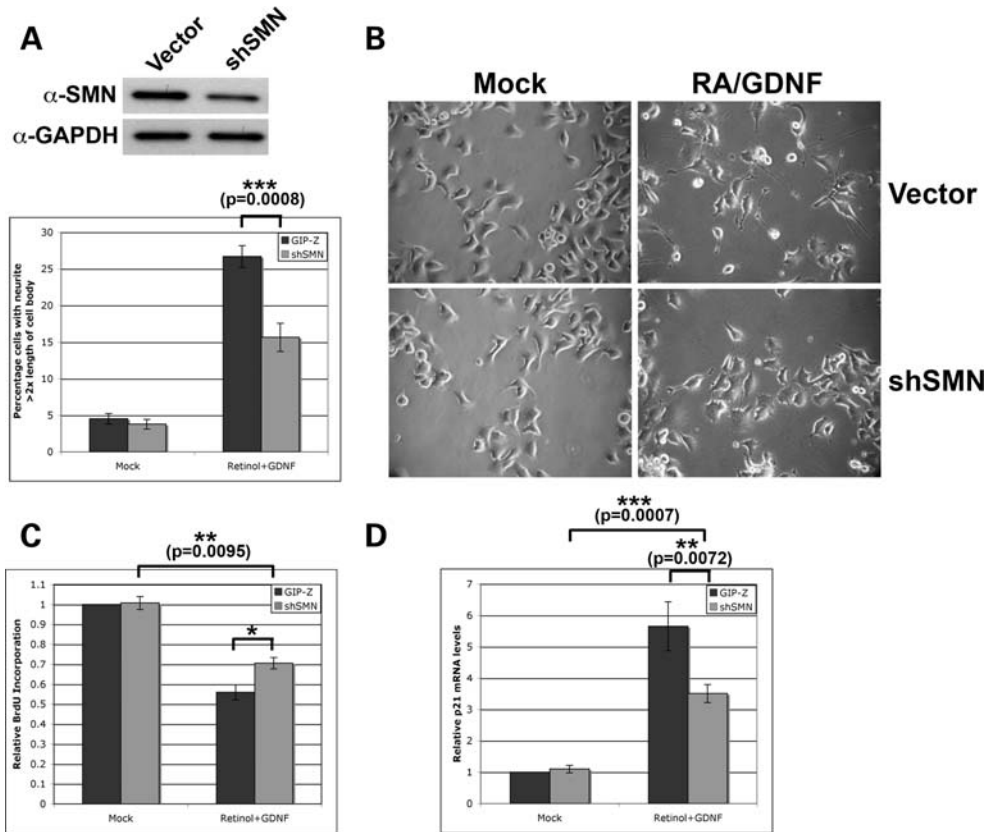


Figure 7. MN-1 cells with reduced SMN levels exhibit various differentiation defects. Representative western blot showing reduced SMN expression in a stable cell line expressing an shRNA targeting SMN mRNA 3'UTR. shSMN cultures showed fewer cells with long neurites following treatment with differentiation media in comparison to cells transfected with empty vector control. Bar graph (bottom) shows average percentage of cells with long neurites ($>2\times$ length of cell body) \pm SD ($n = 4$; 20 fields per experiments) (A). Representative phase-contrast images showing reduced differentiation phenotype following RA/GDNF treatment in shSMN cultures relative to empty vector control (B). In maintenance media, the proliferation of SMN knockdown cells is not altered, as determined by measuring BrdU incorporation \pm SD, normalized to undifferentiated (Mock) empty vector control (GIPZ). Addition of differentiation media to SMN knockdown cells slightly reduced proliferation, but not to the same extent as in cells transfected with empty vector ($n = 3$) (C). p21 mRNA induction following differentiation was not as extensive in shSMN knockdown cultures relative to control cells. Bar graph shows relative p21 mRNA levels \pm SD, normalized to undifferentiated empty vector control, as determined by RT-qPCR ($n = 3$) (D). Statistical significance is indicated above respective bar graphs.

whether SMN may influence HuD function in neurites. Control (empty vector) and shSMN knockdown MN-1 cultures were induced to differentiate using RA/GDNF treatment for 48 h. Cytoplasmic extracts from Mock and differentiated cells were then resolved through sucrose density gradient fractionation (Fig. 8). It was previously reported that the 'heavy' fraction at the bottom of the gradient actually contains RNA granules (99). In order to validate this approach, we first probed our fractions using a series of well-accepted markers for mRNPs (Tubulin), ribosomal subunits (rRNA, top panel) and RNA granules (KSRP and HuD), which allowed identification of those respective fractions in the sucrose gradients (Fig. 8A, respective panels). As an indication that fractions 11–13 indeed contained RNA granule components, we observed accumulation of KSRP and HuD in these fractions upon differentiation of control MN-1 cells (Fig. 8A, respective panels). In contrast, no accumulation of either HuD or KSRP was observed in heavy sucrose gradient fractions when MN-1 shSMN cultures were induced to differentiate (Fig. 8A, right, respective panels). These results suggest that SMN is required for proper recruitment of HuD (and KSRP) in dense neuronal RNA granules. Interestingly, SMN was also detected in RNA

granules, which is consistent with its interaction with HuD (and KSRP) in punctate foci in neurites (see Fig. 8A).

Reduced translocation of β -actin mRNA to neuritic processes and growth cones has been observed in SMN-depleted cultured neuronal cell lines and primary motoneurons derived from SMA model mice (21,93). However, to date, no other mRNAs have been documented to be mislocalized in axons of SMA motoneurons. As we found HuD to be misregulated in shSMN knockdown MN-1 cells, we next wanted to assess whether this also impacted on some of its known axonal mRNA targets. The same approach as above was used except that total RNA was extracted from each collected fraction, which was then subjected to RT-PCR to monitor the distribution profiles of specific HuD mRNA targets (Fig. 8B). As a positive control to validate the procedure, the profile of β -actin mRNA was first assessed. As expected, β -actin mRNA was enriched in heavy fractions 11–13 following differentiation of control cells, whereas this redistribution was not observed in the shSMN knockdown samples (Fig. 8B, β -actin panels). Importantly, γ -actin mRNA, which does not translocate into neurites, was not detected in the heavy fractions under any conditions (Fig. 8B, γ -actin

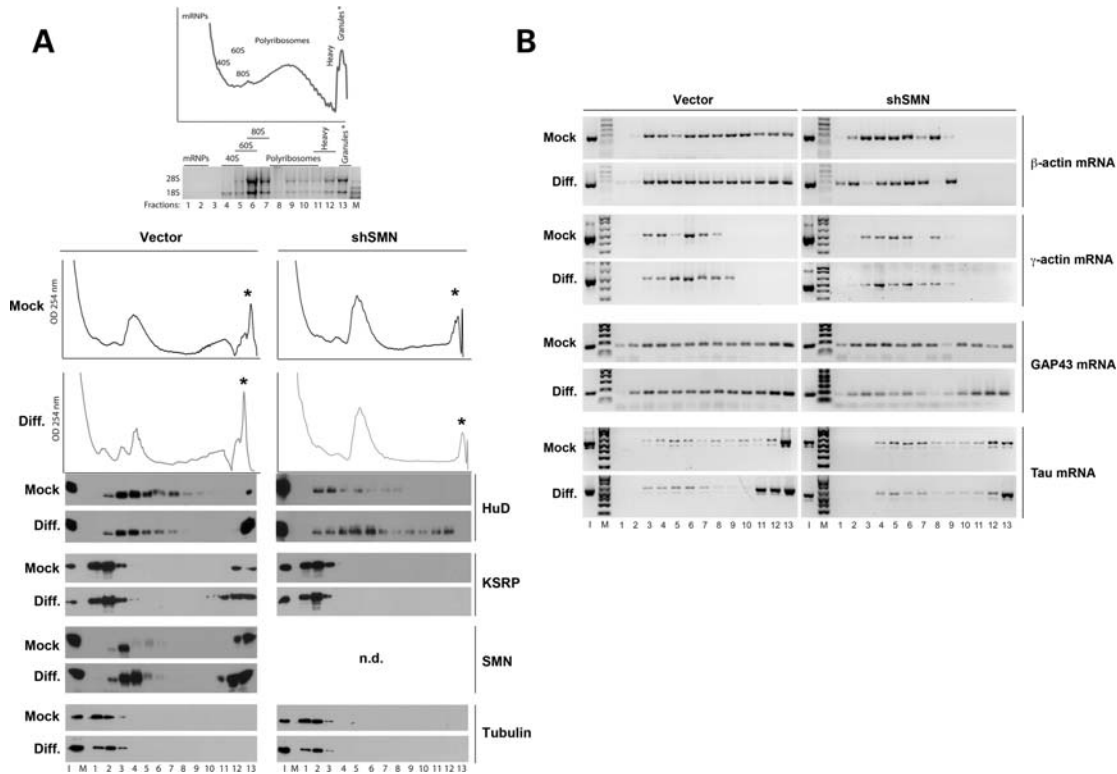


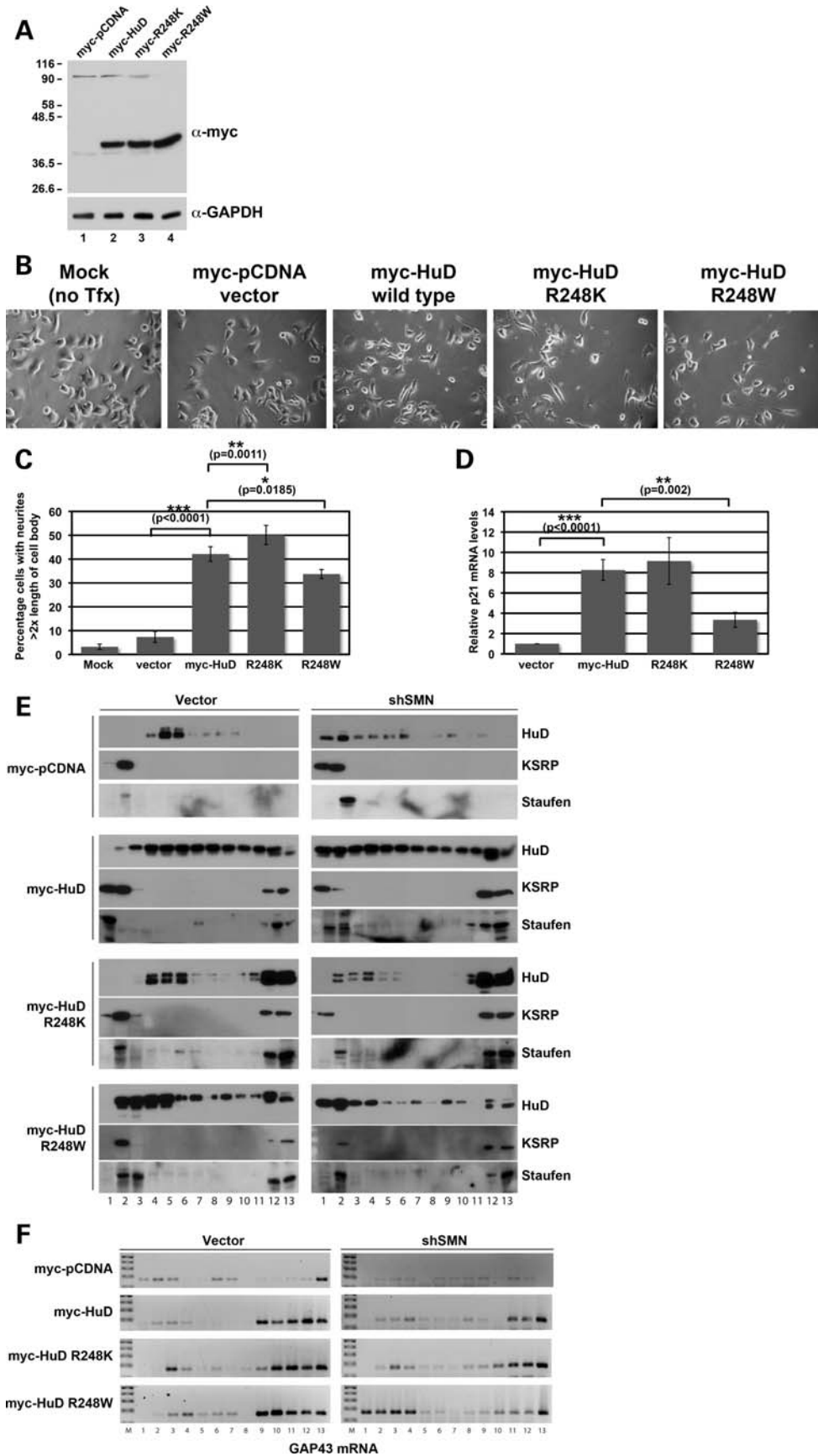
Figure 8. SMN is required for localization of HuD and its mRNA targets into RNA granules. Sucrose density gradient centrifugation was used to fractionate cytoplasmic extracts from empty vector control (Vector) or shSMN cultures, left undifferentiated (Mock) or treated with RA/GDNF for 48 h (Diff.). A representative profile obtained using this approach is shown (top panel). Known constituents of various fractions are indicated above the UV tracing. Those include mRNA ribonucleoprotein particles (mRNPs), small and large ribosomal subunits (40S and 60S), monosomes (80S), polyribosomes and dense RNA granules (*). Total RNA was extracted from each fraction to determine the boundaries between small and large ribosomal subunits. Migration of 28S and 18S ribosomal RNAs is indicated. Representative UV tracings show a relative induction in the RNA granule fractions (*) upon differentiation of Vector-transfected control cultures. This is not observed in the shSMN cultures. Total proteins were extracted from each fraction, resolved by SDS-PAGE, and subjected to immunoblotting with the indicated antibodies. RNA granule components HuD and KSRP are seen enriched in fractions 11–13 upon differentiation of Vector-transfected control cultures (left panels), but not in the context of low SMN levels (right panels). SMN is also detected in the RNA granule fractions, whereas tubulin is only seen in mRNPs, as expected (A). The same approach was used except that total RNA was prepared from each fraction, and RT-PCR was performed using primers to amplify the indicated mRNAs (B).

panels), confirming that we are able to discriminate between cytoplasmic and neuritic RNA granules' mRNA populations. The same fractions were next probed using RT-PCR to examine the distribution profiles in the sucrose gradient fractions of two known HuD targets, namely GAP43 and Tau. GAP43 mRNA was distributed more or less evenly in the gradient under Mock conditions and became more enriched in the heavy fractions following differentiation of MN-1 control cells (Fig. 8B, Vector, Mock and Diff. GAP43 panels). Although still detectable, this shift towards the dense RNA granule fractions was less pronounced in the absence of SMN (Fig. 8B, shSMN, Mock and Diff. GAP43 panels). Tau mRNA, on the other hand, was found largely enriched in the RNA granules fraction (lane 13), even in the absence of differentiation cues, although an even greater accumulation was seen in fractions 11–13 after RA/GDNF treatment (Fig. 8B, Vector, Mock and Diff. Tau panels, respectively). Again, this enrichment of Tau mRNA in the RNA granule fractions was greatly reduced in the MN-1 shSMN knockdown samples (Fig. 8B, shSMN, Mock and Diff. panels). These results indicate that the defect in HuD recruitment to RNA granules observed in the face of reduced SMN expression impacted

on the fate of HuD mRNA targets GAP43 and Tau. This also constitutes the first identification of additional axonal mRNAs that are misregulated in SMA-like conditions.

Overexpression of HuD can rescue SMA-like motoneuron defects

HuD overexpression was very effective at promoting differentiation of motoneuron-derived MN-1 cells, even in the absence of any additional stimuli (see Fig. 6), suggesting that HuD acts downstream of normal differentiation cues and is sufficient to induce both cell-cycle exit and neurite extension. Thus, we reasoned that this may constitute a viable strategy to rescue neuronal defects observed in SMA-like conditions. Furthermore, these experiments should also help clarify where SMN is situated within the regulatory pathway characterized in the current study (i.e. RA/GDNF–CARM1–HuD–mRNA targets–neuronal differentiation). To verify this hypothesis, wild-type and R248 mutant alleles of HuD were overexpressed in shSMN knockdown MN-1 cells (Fig. 9A), as described above for parental MN-1 cultures. Strikingly, both wild-type and mutant HuD proteins were able to induce neurite



extension in shSMN knockdown cultures (Fig. 9B), albeit to varying extent, R248K being the most efficient and R248W the least (Fig. 9C). Moreover, as was seen for wild-type MN-1 cells, both myc-HuD and myc-HuD-R248K were able to induce an ~8-fold upregulation in p21 mRNA levels, whereas the R248W allele had no significant effects over the empty vector control (Fig. 9D). In order to determine whether HuD overexpression would also be able to somehow rescue proper recruitment to neuronal RNA granules, we again made use of the sucrose gradient fractionation approach. Wild-type and mutant myc-HuD expression vectors were transfected in control and shSMN cell lines as before and cytoplasmic extracts were fractionated on sucrose density gradients as in Figure 8. Strikingly, overexpression of either wild-type or R248 mutant alleles of HuD resulted in a drastic accumulation of RNA granule markers Staufen and KSRP in the heavy fractions, relative to empty vector control transfections (Fig. 9E, respective panels, lanes 11–13). Myc-HuD overexpression was also able to promote recruitment of endogenous HuD to RNA granules, in both control and shSMN cells (Fig. 9E, HuD panels, lanes 11–13). Finally, a similar effect was seen for translocation of GAP43 mRNA into RNA granules (Fig. 9F). Taken together, these results indicate that HuD likely acts downstream of SMN in regulating motoneuron differentiation and, most importantly, shows that it is possible to rescue SMA-like axonal defects through upregulation of RNA-binding protein HuD.

DISCUSSION

We report here a novel interaction between the SMN Tudor domain and neuronal ELAV family protein HuD, in the cytoplasm and neurites of motoneuron-derived MN-1 cells. Importantly, this interaction is completely abolished by mutations found in human patients affected with severe Type I SMA, underscoring its functional relevance for the etiology of the disease. We also demonstrate the existence of a regulatory pathway downstream of retinoid and neurotrophic signaling in MN-1 cells, leading to downregulation of CARM1 expression and resulting in a relative increase in the pool of unmethylated HuD. This change in the methylation status of HuD in turn modulates its binding affinity toward specific mRNA targets, including p21 mRNA, and may also regulate its interaction with the Tudor domain of SMN. Together, our results suggest a dual mode of regulation for HuD in motoneurons: (i) arginine methylation of HuD R248 by CARM1 mainly serves as a regulatory switch to modulate the landscape of mRNA targets that HuD binds and regulates and (ii) SMN mediates the proper translocation of HuD into neuritic RNA granules along with its mRNA targets. Finally, we provide

evidence that upregulation of HuD in motoneurons might be a viable therapeutic strategy for SMA.

HuD interacts with the Tudor domain of SMN

Although SMN has been observed in dendrites, axons and growth cones of neuronal cells (23,24,26,100), the precise nature of the granular foci where it resides in neuronal processes remains unclear. More recent studies have demonstrated that SMN colocalizes with ribosomal RNA, poly(A⁺) mRNAs and PABP in axons of neurons in culture (25,101), which has prompted speculations that it might be a component of neuronal RNA granules. In support of this suggestion, SMN was shown to colocalize with hnRNP Q and hnRNP R in axonal processes (22), and in differentiating PC12 cells, SMN cooperates with hnRNP R to promote neurite outgrowth and proper localization of β -actin mRNA to growth cones (21). Furthermore, our laboratory has recently documented the interaction of SMN with KSRP (29), another known component of the β -actin mRNP (102) as well as neuronal RNA granules (96). We report here a novel interaction between SMN and HuD, a general regulator of post-transcriptional processes in neurons, that has also recently been identified in a proteomic analysis of RNA granule components (96). HuD and KSRP share a number of characteristics in addition to their localization to neuronal RNA granules. First, they both regulate mRNA stability through specific interactions with ARE-containing 3'UTRs and share a number of mRNA targets, including p21^{cip1/waf1} (72,103). Secondly, HuD and KSRP are both methylated by CARM1, at sites flanked by sequences rich in proline, glycine and methionine (PGM) motifs (29,61), a feature recently identified in other CARM1 substrates (e.g. SmB and CA150) that interact with SMN through its Tudor domain (54). Similar to what we observed for KSRP and CA150, CARM1 methylation can enhance binding of HuD to the Tudor domain of SMN (see Fig. 5E). However, we have not been able to observe this effect in co-IP experiments (data not shown), suggesting that SMN and HuD are likely part of a larger complex in cells, where other proteins may provide additional stabilization. Finally, the apparent stoichiometry of the HuD/SMN interaction is reminiscent of what we observed for the KSRP/SMN co-IPs (29), i.e. it would seem that only a portion of the total SMN pool is likely in complex with HuD or that the interaction is of transient nature. This is consistent with the notion that the SMN complex interacts with a plethora of so-called 'substrates' at any one time. Accordingly, we were also not able to observe the reciprocal co-IP, by using antibodies directed against SMN to perform the IP and then blotting for the presence of HuD (data not shown), although this could also be

Figure 9. Overexpression of HuD can rescue SMA-like motoneuron defects and normal recruitment of specific components to RNA granules. Representative immunoblot showing equal expression of myc-HuD alleles in MN-1 shSMN cells (A). Representative phase-contrast images showing induced neurite extension in shSMN cells transfected with myc-HuD alleles, relative to shSMN cells incubated with transfection reagent alone (Mock) or empty vector control (myc-pCDNA) (B). Overexpression of HuD wild-type and mutant alleles induces neurite extension in shSMN cells. Bar graph shows the average percentage of cells with long neurites ($>2 \times$ length of cell body) \pm SD ($n = 3$) (C). Overexpression of HuD wild-type and R248K mutant results in p21 mRNA induction in shSMN cells, whereas no effect is observed with HuD R248W. Bar graph shows relative p21 mRNA levels \pm SD, normalized to empty vector control, as determined by RT-qPCR ($n = 3$) (D). Empty vector control cultures or shSMN MN-1 cells were transfected with either myc-pDNA or myc-HuD wild-type and mutant alleles, followed by sucrose density gradient fractionation as in Figure 8. HuD overexpression results in RNA granule markers HuD, KSRP and Staufen now being properly recruited to dense RNA granule fractions, even in the presence of low levels of SMN (right panels, lanes 11–13) (E). The same effect is observed for GAP43 mRNA (F). Statistical significance is indicated above respective bar graphs.

explained by epitope inaccessibility in the context of the complex.

As both HuD and SMN have been detected in granular foci containing RNA, it was important to determine whether their interaction was direct or mediated through an RNA moiety. Intriguingly, we found the interaction to be highly sensitive to RNase treatment when the isolated SMN Tudor domain was used in GST-pull-down experiments, whereas we observed no effect on co-IPs of the two proteins (Fig. 1C and data not shown, respectively). In contrast, the interaction between SMN and KSRP was completely independent of the presence of RNA, regardless of the technique used (see Ref. 29, and Fig. 1B). This discrepancy does not exclude the possibility that SMN and HuD might interact in the context of an mRNP complex, as assembly of a stable multiprotein complex may preclude accessibility to nucleases. Nevertheless, we have shown that HuD and the Tudor domain of SMN can interact directly, using a blot overlay approach (Fig. 1E). Intriguingly, this interaction seems to occur mostly with a slower-migrating HuD species (indicated with an arrow in Fig. 1E), which is something we also observed using the full-length SMN protein in GST-pull-down assays (e.g. see Fig. 1D, lane 3). The precise nature of this slower-migrating form of HuD is discussed below. Physical interaction, in cells, is also supported by our BiFC experiments, where we can observe reconstitution of the YFP molecule in both the cytoplasm and, as punctate foci, in neurites of cultured motoneuron-derived MN-1 cells (Fig. 2).

SMN mediates recruitment of HuD and its mRNA targets in neuronal RNA granules

Despite accumulating evidence for the association of SMN with RNA granule components, the function it might play in the axonal compartment remains largely unknown. Based on its well-characterized function in promoting the assembly of snRNP particles in the cytoplasm (see Introduction), it was proposed that SMN may also serve a similar role for axonal mRNP complexes (1,104,105). This is consistent with the observation that, in axons, SMN still colocalizes with Gemins (37,38), which are intrinsic components of its activity as a chaperone for snRNP assembly (9 and references therein). More recently, it has been shown that pICln, a component of the PRMT5 complex which methylates snRNP Sm proteins, is also a key player in the SMN chaperone assembly mechanism (106), although its presence in axons has never been investigated. We have used sucrose density gradient centrifugation to obtain fractions containing dense RNA granules, an approach first developed and validated by Krichevsky and Kosik (99). Using this strategy, we demonstrated that SMN is required for efficient transfer of HuD and KSRP into dense RNA granules upon differentiation of motoneuron-derived MN-1 cells (Fig. 8A). Accordingly, selected HuD mRNA targets that are known to be transported in axons are also misregulated in the face of reduced SMN expression (Fig. 8B). Together, these results suggest that SMN indeed could promote assembly of neuronal RNA granules, although further experimentation will definitely be required to assess this more directly and gain more insights into the precise molecular mechanism involved.

Although SMN can bind RNA *in vitro* (107,108), it was never shown to actually interact directly with mRNAs in cells. Nevertheless, we cannot exclude the possibility that it may play a more functional role in RNA granules. For example, it could modulate the activities of its RNA-binding protein partners through its chaperoning of protein–protein or protein–RNA interactions. Those processes associated with RNA granules include mRNA transport, localized mRNA stability and translational regulation. Defects in localization of β -actin at growth cones have been seen in SMA motoneurons (21), and we document here reduced recruitment to RNA granules of HuD mRNA targets GAP43 and Tau, in the face of low SMN expression. As mentioned above, we have also reported aberrant mRNA stability of p21 mRNA in mild SMA model mice (29). We have not observed an increase in p21 mRNA steady-state levels in our MN-1 shSMN knockdown cultures (see Fig. 7D). This either reflects differences between *in vitro* and *in vivo* models or could suggest that the observed increase in p21 levels originated from a distinct cell type (i.e. not motoneurons) in spinal cord tissues. Finally, misregulation of translation has never been observed in SMA cells as of yet. However, it was recently reported that HuD can stimulate cap-dependent translation, through a novel interaction with eIF4A, and that this might explain at least in part how HuD triggers the induction of neuronal differentiation (109). Hence, it will be interesting to explore a potential role of SMN in this process in future studies.

Identification of a regulatory pathway involving CARM1 and HuD in motoneurons

A previous study (61) uncovered a regulatory pathway involving CARM1 and HuD implicated in the NGF-stimulated differentiation of rat PC12 cells. Because of our finding that SMN interacts with HuD, we have now confirmed the existence and investigated in greater detail this regulatory pathway in motoneuron-derived MN-1 cells. First, we have found that CARM1 expression is downregulated, at the protein level, following treatment of MN-1 cells with *trans*-retinol and neurotrophic factors (Fig. 4C). This is indicative of regulation at the level of either translation and/or protein turnover. The precise mechanism involved in this downregulation remains unknown, but we have observed in preliminary experiments that MG132 induced a stabilization of CARM1 (G. Sanchez and J. Côté, unpublished data), suggesting that proteosomal degradation may at least participate in the process, although further experiments will be required to clarify this issue. In contrast to CARM1 levels, HuD expression remained mostly constant during MN-1 differentiation, suggesting that it is likely protein turnover in the absence of CARM1 activity that eventually leads to a relative increase in the pool of unmethylated HuD. Another alternative to explain a reduction in HuD methylation would be to invoke the contribution of an arginine demethylase. The only protein arginine demethylase described to date is JMJD6 (110), although it was later debated in a subsequent study that this enzyme catalyzed lysyl hydroxylation of splicing factor U2AF65 (111). In any case, a reduction in HuD methylation was observed in our *in vitro* methylation assays using

differentiating extracts as a source of enzyme (Fig. 4B), and the conditions used for these assays should not be permissive to demethylase activity according to the proposed chemistry for these enzymes (110). One of the antibodies used in the present study to detect HuD actually recognizes two bands in immunoblots (e.g. see Fig. 4C, anti-HuD panel). We have confirmed that both bands originate from HuD mRNAs because they both can be downregulated using an shRNA targeting HuD 3'UTR sequences (Hubers *et al.*, unpublished results). Hence, they likely represent alternatively spliced isoforms of HuD or they result from post-translational modification(s). Intriguingly, in extracts where CARM1 expression has been reduced through RNA interference, this antibody only picks up the faster-migrating band in immunoblots (e.g. see Fig. 4C, lane 6, anti-HuD panel). As we have previously reported that CARM1 can regulate alternative splicing of at least some pre-mRNAs (54), we verified whether this was what we were seeing here. Using RT-PCR, with primers flanking alternative exons 6 and 7 in HuD pre-mRNA, we failed to see any difference in the relative ratio of splicing isoforms between Mock and CARM1 knockdown cells (data not shown). Thus, our preliminary experiments suggest that this difference may reflect co-regulation between arginine methylation and another post-translation modification, such as, e.g. phosphorylation, which is known to occur in the vicinity of R248 in the HuD hinge region (see 64 for a review).

CARM1 emerging as a master regulator of the proliferative/differentiation switch

Results obtained with mice carrying a targeted deletion of *Carm1* have demonstrated the importance of CARM1 in promoting the differentiation of a number of cell types including T-cells, adipocytes and pulmonary epithelial cells (57,112–114). In contrast, other studies have provided evidence in support of a crucial role for CARM1 in maintenance of the proliferative state for neuronal cells (61 and the present study), chondrocytes (115) as well as maintenance of the pluripotency in mouse ES cells (116,117). In most cases, it is through its well-characterized activity as a transcriptional regulator that CARM1 exerts these effects. For example, it was found to associate with *Oct4* and *Sox2* promoter regions to stimulate their expression through modification of histone H3 R17/26 and promote maintenance of pluripotency in mouse ES cells (117). Nevertheless, a few recent studies suggest that CARM1 can also regulate cellular proliferation and differentiation through modulation of post-transcriptional processes (116,118). Of particular relevance to the present work, Calvanese *et al.* (116) have uncovered a novel regulatory pathway in human ES cells, whereby CARM1 methylation of HuR increases its affinity for the mRNA of SIRT1, thus promoting its stabilization and resulting in silencing of key developmental genes by SIRT1. This mechanism is highly reminiscent of the pathway explored here in motoneuron-derived MN-1 cells, except that HuD is targeted downstream of CARM1 and that, importantly, HuD methylation results in reduced binding to specific mRNA targets (see below). It remains unknown whether CARM1 transcriptional activity will also contribute to its role in regulating the proliferation/differentiation switch in neuronal cells. Finally, it is known

that PRMT1 expression in mouse brain is downregulated during embryonic development, whereas PRMT3 and PRMT8 expression go up (119,120), so it will be interesting to investigate further their potential implication in the regulation of neuronal differentiation.

CARM1 regulates HuD RNA binding to specific targets

As mentioned above, previous experiments using IP/RT-PCR suggested that CARM1 methylation of HuD may regulate its association with p21 mRNA (61), although this approach is mostly semi-quantitative and is not necessarily indicative of a direct effect. As the effect of CARM1 on RNA binding had never been explored before (the study discussed above from Calvanese *et al.* was published during the preparation of this manuscript), we wanted to address this in more details. First, using RNA mobility shift assays with purified GST-HuD, we observed a drastic reduction in RNA binding to p21 mRNA ARE sequences when our protein preparation was pre-methylated with CARM1 (Fig. 5A). We were then able to quantify this effect using filter-binding assays and found that HuD methylation by CARM1 results in a ~3-fold reduction in apparent K_d for the 3'UTR fragment of p21 mRNA (Fig. 5B). It is intriguing, at least mechanistically, that CARM1 methylation of the same conserved residue in two highly related ELAV family proteins (HuD and HuR) results in opposite effects on RNA-binding activity. Our very limited assessment of other known HuD targets has shown that this effect can be extended to GAP43 but not to Tau and Nova-1 mRNAs (Fig. 5C), although these results will have to be confirmed as we have done here using more quantitative biochemical approaches. Taken together, these results suggest that methylation of HuD (and likely all other ELAV family members) by CARM1 has the potential to completely remodel the landscape of mRNA targets that it regulates following a specific extracellular cue, without the need to modulate its expression, which brings a whole new level of complexity.

HuD R248 methylation mainly acts as a regulatory switch for cell-cycle exit

We have used mutagenesis to demonstrate that arginine methylation of R248 in HuD can regulate its activity in neuronal differentiation (Fig. 6). Surprisingly, our experiments show that this regulatory switch seems to be most effective in controlling the activity of HuD in promoting cell-cycle exit, through stabilization of p21 mRNA. Specifically, a mutation predicted to mimic arginine methylation (R248W) completely abrogates the effect of HuD overexpression on p21 mRNA levels (Fig. 6F). In contrast, when the same mutants were tested for their capacity to induce neurite extension, only minimal differences between wild-type HuD and both mutant alleles were observed (Fig. 6E). Together, these results are consistent with a model where (i) arginine methylation of R248 by CARM1 would act as an on/off switch for the activity of HuD early in differentiation, in promoting cell-cycle exit, whereas (ii) SMN would be responsible for translocation of HuD into neuronal processes and thus of its role in neurite extension. Nevertheless, we cannot exclude the

potential interference by endogenous wild-type HuD in these experiments, so that differences with mutants might be exacerbated on a HuD null or hypomorphic background. Finally, the presence of other neuronal ELAV family members HuB and HuC in MN-1 cells may also compensate for overexpression of mutant HuD proteins. This would again seem to affect mostly neurite extension assessment.

HuD overexpression can rescue SMA-like motoneuron defects

Strikingly, when the same experiments were performed in our MN-1 *Smn* hypomorph line, overexpression of HuD was still able to strongly induce neuronal differentiation, as monitored through assessment of neurite extension and p21 mRNA upregulation (see Fig. 9A–D). Moreover, HuD was also capable of offsetting the defect observed in recruitment of specific components to RNA granules in SMN knockdown cells (Fig. 9E and F). This would place HuD downstream of SMN (or at least at the same level) in the pathway regulating motoneuron differentiation. It is conceivable that the increased pool of HuD in these experiments may be able to recruit enough SMN toward promoting the assembly of RNA granules to rescue differentiation defects normally observed in the face of reduced SMN expression. Together, these results indicate that low levels of SMN in motoneurons do not result in irreversible defects, at least in a cell culture model. Obviously, many questions now remain to be addressed using SMA model mice, such as, e.g. the viability of this approach in the human SMA genetic background, where very low levels of SMN are often found, along with the presence of SMN Δ 7. It would also be important to determine the ideal window where HuD overexpression might be beneficial. Nevertheless, these results open the door for conception of novel strategies for this devastating disease.

MATERIALS AND METHODS

Cell culture

Motoneuron-derived MN-1 cells were a kind gift of Matthew Butchbach and Arthur Burghes (Ohio State University) and were maintained and induced to differentiate essentially as described previously (29), except that serum was reduced to 2%, and 10 ng/ml GDNF (PeproTech, Rocky Hill, NJ, USA) was added in the differentiation media. To generate a stable knockdown of CARM1 in MN-1 cells, a target sequence was selected using the online 'RNAi Explorer' design algorithm (<http://www.genelink.com/sirna/shRNAi.asp>), and from this, the following two oligos (Sens mCARM1 oligo: 5'-GATCGGCTACATGCTCTTCAATGAACGAATGCTCTCAA-GAGGAGCATTCTTCATTGAAGAGCATGTAGCTTTTTGA; Antisense mCARM1 oligo: 5'-AGCTTCAAAA AAGCTACATGCTCTTCAATGAACGAATGCTCCTCTTGAGAGCATT-CGTTTCATTGAAGAGCATGTAGC) were hybridized, digested and subcloned into the *Bam*H1 and *Hind*III sites of the pRS shRNA vector (OriGene). For the SMN stable knockdown, a pre-designed, microRNA-adapted shRNA lentiviral vector targeting a sequence in the 3'UTR of mouse SMN mRNA (GIPZ #RMM4431, OpenBiosystems)

was used. The pRS-1 (Origene) and pGIPZ (OpenBiosystems) empty vectors, respectively, were used as controls for the selection process. Lipofectamine 2000 (Invitrogen) was used for DNA transfections according to the manufacturer's instruction. Selection was achieved using 4 μ g/ml of puromycin dihydrochloride (Sigma). Pools obtained following 2 weeks of selection regimen were then maintained in 2 μ g/ml of puromycin.

siRNA transfections

Transient knockdown of CARM1 expression using RNA interference was performed as described previously (29). Accell siRNA oligonucleotide duplexes were purchased from Dharmacon for targeting mouse *Carm1* 3' UTR (NM_021531) in MN-1 cells. The siRNA sequences from Accell set of 3 EQ-048766-00-002 are:

siRNA A-048766-13: CUCCUGUCCAUCAGUAAUA,
siRNA A-048766-14: GCAUAGAAAAUAAAAGUGU,
siRNA A-048766-15: CAAGAACCUCAAAGAUCU.

siRNAs were used at 1 μ M final concentration and were transfected following the Accell siRNA Delivery Protocol (according to the manufacturer's instructions). Briefly, MN-1 cells were plated at 25% confluency in Accell siRNA Delivery Media (Accell siRNA Delivery Media B-005000-500) supplemented with 10% FBS at 37°C with 5% CO₂ overnight. After 16–24 h, growth media was removed and the siRNA was added to the cells with a final concentration of 1 μ M in Accell siRNA Delivery media supplemented with 1% FBS. Cells were incubated at 37°C with 5% CO₂ for 72 h. For the rescue experiments, cells were first transfected with 1 μ g of N1-GFP-CARM1 (a gift from Dr Mark Bedford, University of Texas) using LIPOFECTAMINE 2000 (according to the manufacturer's instructions). Approximately 8–12 h after transfection, the same procedure outlined above was followed for delivery of the Access CARM1 siRNAs. Alternatively, our initial siRNA was transfected as described in Ref. (29). Cells were incubated at 37°C with 5% CO₂ for 72 h.

Antibodies

Murine hybridomas producing a monoclonal antibody (mAb) to KSRP were described elsewhere (29) and were either used as tissue culture supernatant (1:5) or purified over a Protein A Sepharose column (Sigma) following the manufacturer's instructions and then used at 1:1000. The 9E10 anti-myc mAb was from the American Type Culture Collection (Manassas, VA, USA). Mouse mAb antibodies against HuD were either from Santa Cruz Biotechnology or Clonogen LLC (clone 16C12) and were used at 1:1000. The anti-SMN mAb (BD Transduction Laboratory, Palo Alto, CA, USA) was used at 1:3000. The anti-CARM1 rabbit polyclonal Ab (Bethyl Laboratory, TX, USA) was used at 1:2000, whereas the anti-GAPDH mAb (Covance, CA, USA) was used at 1:5000. Rabbit polyclonal antibody against p21 was from Santa Cruz Biotechnology (p21/c-19:sc-397) used at 1:1000. The anti-GST rabbit polyclonal Ab was a generous gift from Dr Stephane Richard (Lady Davis Institute, McGill

University). The anti-H3R17me2a mAb (Millipore #07-214) was used at 1:1000. Anti-alpha-Tubulin mouse mAb B512 (Abcam, Cambridge, MA, USA) was used at 1:10 000. The anti-Staufen rabbit polyclonal antibody ab734378 (Abcam) was used at 1:300. Horseradish peroxidase-conjugated goat anti-mouse and goat anti-rabbit secondary antibodies (MP Biomedicals, Solon, OH, USA) were used at a dilution of 1:20 000 and 1:1000, respectively.

Immunoprecipitation and immunoblotting

Proteins were extracted from cells collected from 100 mm plates. Cells were first washed in phosphate-buffered saline (1× PBS) and then incubated in lysis buffer containing 10 mM Tris-HCl, pH 7.4, 150 mM NaCl, 1% Triton, and complete protease inhibitor cocktail (Roche Applied Sciences) with continuous agitation for 30 min at 4°C to ensure complete lysis. Cell extracts were cleared by centrifugation at a maximum speed for 10 min 4°C. Protein concentration was determined by Bradford assay according to the manufacturer's protocol (BioRad, Mississauga, Ont., Canada). Following quantification, equal amounts of each sample was combined with Laemmli reducing buffer (25% glycerol, 125 mM Tris-HCl, pH 6.8, 4% SDS, 700 mM β-mercaptoethanol, 0.1% bromophenol blue) and heated at 95°C for 10 min. Proteins were resolved by 12.5% SDS-PAGE and transferred onto an Immobilon-P polyvinylidene difluoride (PVDF; Millipore: 0.45 μm pores) membranes and then 5% non-fat milk in PBS containing 0.05% Tween-20 (PBS-T) was used to block the membrane for 1 h at room temperature. Membranes were next incubated with primary antibody diluted in 2% non-fat milk in 0.05% PBS-T and 0.02% sodium azide at room temperature for 1 h or at 4°C overnight, then washed three times for 5 min in PBS-T. The secondary antibody was diluted in 2% non-fat milk in PBS-T and then incubated with the membrane for 1 h at room temperature, followed by three further washes in 0.05% PBS-T. Bands were detected using chemiluminescent HRP substrate (Millipore Corporation, Billerica, MA, USA) and exposure to film (Clonex). For IPs, cells were lysed in radioimmunoprecipitation assay (RIPA) buffer [1× PBS, 1% Nonidet P-40, 0.5% sodium deoxycholate, 0.1% SDS, complete (Roche, Laval, Que., Canada) protease inhibitors]. After centrifugation to pellet cellular debris, cell extracts were pre-cleared with 50 μl of 50% protein A-Sepharose slurry. Cleared supernatants were collected, and protein concentration was determined. Immunoprecipitation was routinely performed using 700 μg of total protein per IP and incubating the primary antibody 1 h to overnight with constant end-over-end mixing at 4°C. Fifty microliters of 50% Protein A/G-PLUS Sepharose (Santa Cruz Biotechnology: sc-2003) slurry were then added and samples incubated at 4°C for 1 h with end-over-end mixing. Beads were washed four times with lysis buffer and once with 1× PBS. RNase A treatment was performed as described previously (29). Incubation of the cell lysate at 4°C without RNase A was performed as mock treatment. Protein samples were resolved by SDS-PAGE and transferred to PVDF or nitrocellulose membranes for analysis by immunoblotting with the respective antibody.

GST-pull-down assays

GST, GST-SMN FL, GST-SMN-E134K FL, GST-SMN Tudor, E134K, Q136E, I116F and A111G mutants were purified as described previously (29,49). For GST pull-down assays, fusion proteins were not eluted from the GST beads to allow for simplified collection in pull-downs and resuspended in 50% slurry in 1× PBS supplemented with Complete™ (Roche, Laval, Que., Canada) protease inhibitor cocktail. Protein extracts were prepared from MN-1 cells using 1% triton lysis buffer and were quantified by Bradford assay. For each pull-down, 400–700 μg of the extracts diluted up to 1 ml in lysis buffer was incubated with ~1 μg of the respective GST protein on beads. Forty to seventy micrograms (10% of the amount used for pull-downs) of the original protein lysate were stored for later use as a total lysate sample for SDS-PAGE. The remainder was split evenly among each of the pull-downs. The mixtures were tumbled for 2 h at 4°C. Beads were collected by centrifugation at maximum speed for 15 s, and the supernatant was discarded. The beads were washed four times with lysis buffer, tumbled for 5 min and again centrifuged. One final wash was done identically using 1× PBS. Retained proteins were resolved by SDS-PAGE and analysed by immunoblotting with the respective antibody. RNase A treatment was performed as described previously (29).

Tudor blot overlay assay

MN-1 cell lysates were prepared with RIPA buffer as described above, and the cellular proteins were separated by SDS-PAGE and transferred to nitrocellulose membranes at low voltage. The membranes were blocked for 1 h at room temperature in Tris-buffered saline containing 0.5% Tween 20 with 2% non-fat dry milk. The membranes were then incubated with 1.5 μg/ml of purified GST-SMN-Tdr in the same buffer for 16 h at 4°C. The filters were washed in Tris-buffered saline containing 0.5% Tween 20, and the bound GST-SMN-Tdr was visualized by immunoblotting with anti-GST antibodies. The secondary antibody was a goat anti-rabbit conjugated to horseradish peroxidase (ICN Pharmaceuticals) and chemiluminescence was used for protein detection (PerkinElmer Life Sciences).

Methylation assays

GST-SmB, GST-A1 and His-PRMT1v1 used in these assays were purified as described previously (121). For *in vitro* methylation assays, 5 μg of GST-fused substrates were incubated with 25 mM Tris-HCl, pH 7.5, 50 μM S-adenosyl-L-methionine (SAM; Perkin-Elmer) and 0.55 μCi S-[methyl-³H]-adenosyl-L-methionine (³H-SAM; Perkin-Elmer), in the presence of 5 μg of GST-CARM1 or His-PRMT1v1. The reactions were incubated for 2 h at 37°C with frequent mixing. Laemmli reducing buffer was added to stop the reactions, and the samples were heated at 95°C for 5 min. Reactions were then run on 12.5% SDS-PAGE and transferred onto PVDF membrane. The membrane was dried and sprayed with En³Hance reagent (Perkin-Elmer). Bands were then visualized by fluorography, and the

membrane was used for further western blot studies as described beforehand. Alternatively, methylation assays were performed using 25 μg of total protein extracts taken from MN-1 cells as a source of CARM1 enzyme. Extracts were prepared at various time points during differentiation by lysing cells in 0.5 mM sodium phosphate buffer followed by five cycles of sonications for 10 s each on ice.

Proliferation assays and neurite extension

Five thousand cells were plated into each well of a 96-well plate and incubated overnight in 5% CO₂ atmosphere at 37°C. Wells were washed with 1 \times PBS, and media was replaced with either maintenance media or differentiation media. BrdU assays were performed according to the manufacturer's protocol (Millipore Corporation, Billerica, MA, USA). Briefly, BrdU reagent was added 4 h prior to the addition of detection antibody. Plate reading was done at a single wavelength of 450 nm. Cells incubated without BrdU reagent were used as a control. Relative BrdU values were determined through comparison to the mock-treated MN-1 cells. In order to approximate the percentage of cells expressing neurites at least twice the length of the cell body, cells were plated and grown in 10-cm plates and either kept in maintenance media or treated with differentiation media as described above. A minimum of 10 pictures of various areas of each plate were taken using a Canon Powershot G6 camera. Total number of cells in each frame was counted, as well as the cells expressing long neurites. Percentage of cells with these neurites was taken by dividing this number by the total number of counted cells.

Immunofluorescence and phase-contrast microscopy

Prior to plating the cells, coverslips were submerged in NaOH-saturated methanol for 30 min and washed in sterile water followed by ethanol. The coverslips were then dried before incubating them in coating solution containing 100 $\mu\text{g}/\text{ml}$ poly-D-lysine (Sigma-Aldrich, St Louis, MO, USA) and 33 $\mu\text{g}/\text{ml}$ mouse laminin (Sigma-Aldrich, St Louis, MO, USA) overnight in 5% CO₂ at 37°C. The coverslips were then placed in maintenance media for 2 h before plating cells overtop. Cells to be used for differentiation experiments were allowed 24 h to adhere to the coverslips before changing media, followed by a further 48 h incubation. Media was removed and the coverslips were washed twice with 1 \times PBS. Cells were fixed for 5 min at room temperature in a solution comprised of 48% acetone, 47% methanol and 5% formaldehyde, and rinsed three times in PBS. The cells were then permeabilized with 0.5% triton X-100 in PBS at room temperature for 5 min, and subsequently washed three times with 1 \times PBS. Following the washes, the cells were blocked with 1 \times PBS containing 0.1% BSA for 30 min. The selected primary antibody was then placed on the coverslips for 1 h. The coverslips were washed first with 0.1% triton X-100 in PBS, then twice in 1 \times PBS, before incubation with the secondary antibody in the dark for 1 h at room temperature. The cells were again rinsed once with 0.1% triton X-100 in 1 \times PBS and twice in 1 \times PBS prior to mounting the coverslips using Vectashield mounting medium containing DAPI (Vector

Laboratories, Inc.) on glass slides. Imaging was done using a Zeiss Axio Imager.Z1 microscope, where the cells were viewed through a Zeiss 40 \times or 63 \times objective. The AxioCam HRm camera was used for image acquisition. For quantification of colocalization, foci were counted for 20 neurites chosen randomly, and the ratio of foci where both fluorescence signals coincided was expressed as percentage \pm SEM for each fluorophore. Colocalization in the Z-plane was confirmed by acquiring z-stacks using the apotome module for each neurite used for quantification.

DNA plasmids

The section of the 3'UTR of p21 containing the three AU-rich regions found to bind to HuD (72) was amplified using RT-PCR (5'-TCACTCTGTGTGCTTAATTA-3', 5'-AGGACTG TTCCTCCGGTATAGG-3'), treated with Klenow to generate blunt ends and subcloned into pBluescript SK vector (Stratagene) at the *EcoRV* site. First, in order to identify YFP fragments that can associate to form a bimolecular fluorescent complex, we generated the bicistronic expression vectors. The constructs encoding N-YFP (Nyfp-) or the C-terminal fragment of YFP (Cyfp) were generated as follows: The DNA sequence encoding enhanced green fluorescent protein (EGFP) was removed by restriction endonuclease digestion using *NheI* and *BspEI* and replaced with a sequence encoding the N-terminal region (1–154 amino acids: Nyfp) and C-terminal region (155–238 amino acids: Cyfp) of YFP. A linker sequence (RSIAT) was also engineered to prevent disruption of protein folding in the context of the fusion. The Nyfp and Cyfp fragments were generated using PCR with pEYFP-C1 vector (Clontech) as a DNA template and the following primers:

Nyfp-1–154 (5'-gcatgctagcatggtgagcaagggcag-3'
and 5'-atgctccggaagtagcaatagaacgcgatgatagacgttg-3')
Cyfp-155–238 (5'-gcatgctagcatggccgacagcagaagaac-3'
and 5'-atgctccggaagtagcaatagaacggtacagctcgtccatgcc-3').

The *NheI* and *BspEI* sites are underlined and the RSIAT sequence is indicated in bold. These vectors were used for the Bimolecular Fluorescence complementation system (BiFC). The BiFC constructs expressing Nyfp-H/SMN and HuD/SMN-Cyfp were constructed by a two-step subcloning strategy. First, the cDNA encoding HuD was removed from myc-pcDNA-HuD (a gift from Dr Bernard Jasmin, University of Ottawa) digested with *BamHI* and *XhoI*. The resulted DNA fragment was then inserted in the *BglIII* and *SalI* sites of N-YFP and C-YFP, respectively. Wild-type and mutant SMN cDNA sequences were removed from EGFP-C1-SMN (122) by restriction endonuclease digestion following the same strategy as described above.

Bimolecular fluorescence complementation

MN-1 cells were co-transfected using Lipofectamine Plus (Invitrogen, Burlington, Ont., Canada) with a total 1.0 μg of DNA of the respective plasmids using an empirically determined ratio of 2:1 (Nyfp fusion relative to yfpC fusion constructs). Transfected cells were incubated at 37°C for 24–48 h and then fixed with 4.0% paraformaldehyde in PBS and

permeabilized with 0.5% Triton X-100 in 1 × PBS. YFP fluorescence documented using a Z.1 AxioImager upright microscope (Carl Zeiss Canada Ltd, Toronto, Ont., Canada) equipped with proper filters, and images were captured with an AXIOCAM HRM R 2.0 CCD digital camera.

Semi-quantitative RT-PCR and RT-qPCR

Total RNA was isolated from cells using Trizol reagent (Invitrogen, Burlington, Ont., Canada) according to the manufacturer's protocol. Samples were resuspended in diethylene pyrocarbonate (DEPC)-treated water, and the optical density was read on a spectrophotometer at a wavelength of 260 nm. RNA quality was determined by agarose gel electrophoresis. To generate cDNA, 1 µg of the respective RNA was incubated with 1 µM oligo-dT for 10 min at 65°C, followed by reverse transcription using 0.5 mM deoxyribonucleotide triphosphates (dNTPs; Invitrogen), 20 U rRNasin (Promega, Madison, WI, USA) and 10 U AMV reverse transcriptase enzyme (Promega, Madison, WI, USA) in AMV reverse transcriptase buffer (Promega, Madison, WI, USA) for 1 h at 42°C. cDNAs were then used in PCR reactions using specific forward and reverse primers for:

GAPDH: (F) 5'-ACCACAGTCCATGCCATCAC-3'
(R) 5'-TCCACCACCCTGTTGCTGTA-3'
β-actin: (F) 5'-TCTTGGGTATGGAATCCTGTGGCA-3'
(R) 5'-ACTCCTGCTGTGATCCACATCT-3'
γ-actin: (F) 5'-ACAGCTTTACCACCACTGCTGAGA-3'
(R) 5'-ACTCCTGCTGTGCTGATCCACATCT-3'
p21: (F) 5'-CTCTTCTGCTGTGGGTCAGGA-3'
(R) 5'-GTGGGGCAAGTGCCTAGATA-3'
GAP43: (F) 5'-TTTGTCTTCTTGGTGTGTTATGGC-3'
(R) 5'-GAACGGAACATTGCACACACA-3'
Nova-1: (F) 5'-TGAGTGCCCCATTATACGTCAG-3'
(R) 5'-TAAACAAGCATATCATTCCCTTTG-3'
Tau: (F) 5'-GGTCGAAGATTGGCTCTACTG-3'
(R) 5'-GCCAAGGAAGCAGACACTTC-3'
HuD: (F) 5'-ACGCATCTGGTTGATCAAG-3'
(R) 5'-AGGACACTCTCATCAGAATC-3'

PCR products were electrophoresed on 2.0% agarose gels and visualized by ethidium bromide staining. Results were captured on a Kodak Gel Logic 200 gel documentation setup and quantified by using the accompanying Kodak 1D analysis software. For quantitative PCR (qPCR) reactions, 25 ng of cDNA was combined with iQ SYBR Green Supermix (BioRad, Mississauga, Ont., Canada) and 400 nM of the respective forward and reverse primers. Primers used were as follows:

p21: (F) 5'-CAGCGATATCCAGACATTGAGA-3'
(R) 5'-CTCAGACACCAGAGTGCAAGAC-3'
GAPDH: (F) 5'-ACCACAGTCCATGCCATCAC-3'
(R) 5'-TCCACCACCCTGTTGCTGTA-3'
CARM1: (F) 5'-AGCTGTGCAGTACTTCCAGTTCTA-3'
(R) 5'-ATTGTTACTCTTACCAGGACCTC-3'
GAP43: (F) 5'-TTTGTCTTCTTGGTGTGTTATGGC-3'
(R) 5'-GAACGGAACATTGCACACACA-3'

For IP/RT-PCR experiments, cell extracts (equalized for total protein concentration) were incubated overnight at 4°C

with beads and affinity-purified anti-HuD or mouse IgG control antibody. The beads were washed four times with IPP-50 buffer (25 mM Tris-HCl; 50 mM KCl; 2 mM MgCl₂; 1 mM DTT; 0.01% Triton X-100). RNA extraction and cDNA synthesis were then performed as described above.

RNA mobility shift assays

To generate a ³²P-labeled p21 RNA fragment, the p21 plasmid was first linearized using *Eco*RI. 0.5 µg of the linearized template was incubated for 2 h at 37°C in a RNA labeling mixture containing 0.4 mM ATP, 0.4 mM CTP, 0.1 mM GTP, 0.1 mM UTP, 10 mM DTT, 20 U rRNasin (Promega), 20 µCi ³²P-UTP (Perkin-Elmer) and 20 U T7 polymerase (Promega) in T7 RNA polymerase buffer (Promega). Ten units of RQ1 DNase (Promega) were added, and the reactions were incubated for a further 15 min at 37°C. Next, 0.3 M RNase-free NaOAc with 0.2% SDS was combined with the mixture, followed by the addition of a phenol, chloroform and isoamyl alcohol mixture at a ratio of 25:24:1. Reactions were briefly shaken by hand and centrifuged at room temperature for 5 min at maximum speed. The aqueous phase containing the RNA was extracted, ethanol was added to a final concentration of approximately 75% and the tubes were placed on dry ice for 10 min. Reactions were centrifuged for 15 min at 4°C to precipitate the RNA, the supernatant was discarded and the pellet was allowed to air-dry briefly. Following resuspension in DEPC-treated water, the labeled RNA was further isolated using the RNA Cleanup Kit (Qiagen) according to the manufacturer's instructions. Concentration of the radioactive RNA was determined using a scintillation counter in Cerenkov mode. *In vitro* methylation assays were performed as described above except that 100 µM cold AdoMet was used for the reactions. Reactions were performed with either GST-CARM1 or GST alone to generate a methylated and unmethylated GST-HuD, respectively. One, ten or hundred nanograms of methylated or unmethylated GST-HuD protein was incubated with 5 µg/µl of heparin and 2 fmol of ³²P-labeled p21 mRNA in 1 × PBS on ice for 10 min. One microliter of RNA loading dye was added, and samples were loaded and run on a 3.5% (pre-run) bis-acrylamide non-denaturing gel for 2 h. The gel was dried onto Whatmann paper under heat and vacuum, exposed to film overnight and visualized by autoradiography.

Filter-binding assays

Methylated and unmethylated HuD were prepared as described above. Increasing concentrations of HuD were mixed with 2 fmol of ³²P-p21 mRNA in RNA-binding buffer consisting of 10 mM Tris-HCl, pH 7.4, 1.5 mM MgCl₂, 150 mM KCl, 0.5 mM dithiothreitol (DTT), 0.1 mM phenylmethanesulfonyl fluoride and complete protease inhibitor cocktail (Roche Applied Science). Reactions were prepared on ice and incubated for 10 min. The 96-well apparatus containing a nitrocellulose membrane pre-soaked in RNA-binding buffer was assembled. Wells were washed with binding buffer, and vacuum was applied. Following the 10 min incubation, the mixture was applied to the appropriate wells under vacuum and allowed to run through for 5 min.

Wells were washed twice with RNA-binding buffer to remove unbound RNA, and vacuum was applied for 30 min to aid in drying the membrane. The apparatus was disassembled, the membrane was removed and allowed to dry for 1 h before exposure to film for 2 h and visualization by autoradiography.

Site-directed mutagenesis

The pcDNA 3.1 myc-HuD arginine 248 to lysine or tryptophan substitutions were generated using the QuikChange XL Site-Directed Mutagenesis Kit (Stratagene), according to the manufacturer's protocol. The solution used for mutagenesis consisted of 0.2 mM dNTPs, 0.2 μ M of the respective forward and reverse primers, 50 ng of plasmid DNA and 2.5 U Pfu Turbo enzyme in Pfu Turbo buffer (Stratagene).

R248K mutant primers: (F) 5'-CCACCAGGCTCAGAA GTTCAGGCTGGACA-3' and (R) 5'-TGTCCAGCCTGAAC TTCTGAGCCTGGTGG-3'; R248W mutant primers: (F) 5'-C CACCAGGCTCAGTGGTTCAGGCTGGA-3', (R) 5'-TCCA GCCTGAACCACTGAGCCTGGTGG-3'.

The PCR program used began with 95°C for 30 s and was followed with 18 cycles at 95°C for 30 s, 55°C for 1 min and 68°C for 22 min. The sequence ended with 68°C for 10 min. The DNA was then incubated with 20 U DpnI restriction enzyme for 1 h at 37°C before transformation into XL-1 Blue cells. Mutagenesis was confirmed by automated sequencing (StemCore Services, Ottawa) of the full-length HuD cDNA.

Sucrose density gradient fractionation

Cell fractionation of motorneuron-derived MN-1 cells was performed as previously reported (99). Briefly, MN-1 cells from two 150 mm diameter dishes per condition were washed with ice-cold 1 \times PBS and scraped with cold low-salt lysis buffer (20 mM Tris-HCl, pH 7.5, 10 mM NaCl, 3 mM MgCl₂, 1 mM RNasin, 1 mM dithiothreitol, 0.3% Triton X-100 and 50 mM sucrose). Nuclei and the majority of mitochondria were sedimented by centrifugation for 10 min at 10 000g at 4°C. The NaCl and MgCl₂ concentrations in the cytoplasmic extracts (supernatants) were adjusted to 170 and 13 mM, respectively. Linear sucrose gradients (15–45% (w/w) in 25 mM Tris-HCl, pH 7.5, 25 mM NaCl, 5 mM MgCl₂) were prepared using Hoefer Scientific Instruments (San Francisco, CA, USA) gradient maker with a sublayer of 0.5 ml of 45% sucrose bed. One and two-tenths milliliters of the cytoplasmic extracts were overlaid onto 10.6 ml of gradients and centrifuged at 85 784.83g for 2 h at 4°C in SW40 swing out rotor. Fractions of 1 ml volume were collected using a fractions collector (Brandel-Amersham), and their quality was continuously monitored at 254 nm using an ISCO UA-6 UV detector. For RNA and protein isolation, the fractions were precipitated with 0.1 M NaCl and 2.5 volumes of ethanol, respectively. The pellets were dissolved in TRIzol Reagent (Invitrogen, Burlington, Ont., Canada) and RNA and protein were extracted according to the manufacturer's protocol. Purified RNA was resuspended in 30 ml of RNase-free water, and its quality was checked on 1.5% agarose gels. Alternatively, proteins were extracted from the

sucrose fractions by ethanol precipitation. The protein pellets were resuspended in 100 μ l of 2 \times Laemmli buffer.

Statistical analysis

Paired *t*-tests were performed using InStat 3.0 (GraphPad Software), with 95% confidence interval. Two-tailed *P*-values are indicated above each compared pairs.

SUPPLEMENTARY MATERIAL

Supplementary Material is available at *HMG* online.

ACKNOWLEDGEMENTS

We are in debt to Dr Martin Holcik and his team for generously providing assistance with sucrose density gradient fractionation and filter-binding assays. We also wish to thank Dr Laura Trinkle-Mulcahy for her help in designing BiFC constructs and experiments.

Conflicts of Interest statement. None declared.

FUNDING

J.C. is the recipient of a Canada Research Chair (Tier 2) in RNA Metabolism and is supported by operating grant #MOP-86746 from CIHR.

REFERENCES

1. Monani, U.R. (2005) Spinal muscular atrophy: a deficiency in a ubiquitous protein; a motor neuron-specific disease. *Neuron*, **48**, 885–895.
2. Lefebvre, S., Burglen, L., Frezal, J., Munnich, A. and Melki, J. (1998) The role of the SMN gene in proximal spinal muscular atrophy. *Hum. Mol. Genet.*, **7**, 1531–1536.
3. Russman, B.S. (2007) Spinal muscular atrophy: clinical classification and disease heterogeneity. *J. Child Neurol.*, **22**, 946–951.
4. Lefebvre, S., Burglen, L., Reboullet, S., Clermont, O., Burlet, P., Viollet, L., Benichou, B., Cruaud, C., Millasseau, P., Zeviani, M. *et al.* (1995) Identification and characterization of a spinal muscular atrophy-determining gene. *Cell*, **80**, 155–165.
5. Gubitz, A.K., Feng, W. and Dreyfuss, G. (2004) The SMN complex. *Exp. Cell Res.*, **296**, 51–56.
6. Otter, S., Grimmler, M., Neuenkirchen, N., Chari, A., Sickmann, A. and Fischer, U. (2007) A comprehensive interaction map of the human survival of motor neuron (SMN) complex. *J. Biol. Chem.*, **282**, 5825–5833.
7. Carissimi, C., Baccon, J., Straccia, M., Chiarella, P., Maiolica, A., Sawyer, A., Rappsilber, J. and Pellizzoni, L. (2005) Unrip is a component of SMN complexes active in snRNP assembly. *FEBS Lett.*, **579**, 2348–2354.
8. Carissimi, C., Saieva, L., Baccon, J., Chiarella, P., Maiolica, A., Sawyer, A., Rappsilber, J. and Pellizzoni, L. (2006) Gemin8 is a novel component of the survival motor neuron complex and functions in small nuclear ribonucleoprotein assembly. *J. Biol. Chem.*, **281**, 8126–8134.
9. Pellizzoni, L. (2007) Chaperoning ribonucleoprotein biogenesis in health and disease. *EMBO Rep.*, **8**, 340–345.
10. Chari, A., Paknia, E. and Fischer, U. (2009) The role of RNP biogenesis in spinal muscular atrophy. *Curr. Opin. Cell Biol.*, **21**, 387–393.
11. Kolb, S.J., Battle, D.J. and Dreyfuss, G. (2007) Molecular functions of the SMN complex. *J. Child Neurol.*, **22**, 990–994.
12. Wan, L., Battle, D.J., Yong, J., Gubitz, A.K., Kolb, S.J., Wang, J. and Dreyfuss, G. (2005) The survival of motor neurons protein determines

- the capacity for snRNP assembly: biochemical deficiency in spinal muscular atrophy. *Mol. Cell. Biol.*, **25**, 5543–5551.
13. Zhang, Z., Lotti, F., Dittmar, K., Younis, I., Wan, L., Kasim, M. and Dreyfuss, G. (2008) SMN deficiency causes tissue-specific perturbations in the repertoire of snRNAs and widespread defects in splicing. *Cell*, **133**, 585–600.
 14. Gabanella, F., Butchbach, M.E., Saieva, L., Carissimi, C., Burghes, A.H. and Pellizzoni, L. (2007) Ribonucleoprotein assembly defects correlate with spinal muscular atrophy severity and preferentially affect a subset of spliceosomal snRNPs. *PLoS ONE*, **2**, e921.
 15. Bäumer, D., Lee, S., Nicholson, G., Davies, J.L., Parkinson, N.J., Murray, L.M., Gillingwater, T.H., Ansong, O., Davies, K.E. and Talbot, K. (2009) Alternative splicing events are a late feature of pathology in a mouse model of spinal muscular atrophy. *PLoS Genet.*, **5**, e1000773.
 16. Liu, H., Shafey, D., Moores, J. and Kothary, R. (2010) Neurodevelopmental consequences of Smn depletion in a mouse model of spinal muscular atrophy. *J. Neurosci. Res.*, **88**, 111–122.
 17. Champion, Y., Neel, H., Gostan, T., Soret, J. and Bordonné, R. (2010) Specific splicing defects in *S. pombe* carrying a degon allele of the survival of motor neuron gene. *EMBO J.*, **29**, 1817–1829.
 18. Winkler, C., Eggert, C., Grادل, D., Meister, G., Giegerich, M., Wedlich, D., Laggebauer, B. and Fischer, U. (2005) Reduced U snRNP assembly causes motor axon degeneration in an animal model for spinal muscular atrophy. *Genes Dev.*, **19**, 2320–2330.
 19. Burghes, A.H.M. and Beattie, C.E. (2009) Spinal muscular atrophy: why do low levels of survival motor neuron protein make motor neurons sick? *Nat. Rev. Neurosci.*, **10**, 597–609.
 20. McWhorter, M.L., Boon, K.-L., Horan, E.S., Burghes, A.H.M. and Beattie, C.E. (2008) The SMN binding protein Gemin2 is not involved in motor axon outgrowth. *Dev. Neurobiol.*, **68**, 182–194.
 21. Rossoll, W., Jablonka, S., Andreassi, C., Kroning, A.K., Karle, K., Monani, U.R. and Sendtner, M. (2003) Smn, the spinal muscular atrophy-determining gene product, modulates axon growth and localization of β -actin mRNA in growth cones of motoneurons. *J. Cell Biol.*, **163**, 801–812.
 22. Rossoll, W., Kroning, A.K., Ohndorf, U.M., Steegborn, C., Jablonka, S. and Sendtner, M. (2002) Specific interaction of Smn, the spinal muscular atrophy determining gene product, with hnRNP-R and gry-rbp/hnRNP-Q: a role for Smn in RNA processing in motor axons? *Hum. Mol. Genet.*, **11**, 93–105.
 23. Bechade, C., Rostaing, P., Cisterni, C., Kalisch, R., La Bella, V., Pettmann, B. and Triller, A. (1999) Subcellular distribution of survival motor neuron (SMN) protein: possible involvement in nucleocytoplasmic and dendritic transport. *Eur. J. Neurosci.*, **11**, 293–304.
 24. Pagliardini, S., Giavazzi, A., Setola, V., Lizier, C., Di Luca, M., DeBiasi, S. and Battaglia, G. (2000) Subcellular localization and axonal transport of the survival motor neuron (SMN) protein in the developing rat spinal cord. *Hum. Mol. Genet.*, **9**, 47–56.
 25. Zhang, H.L., Pan, F., Hong, D., Shenoy, S.M., Singer, R.H. and Bassell, G.J. (2003) Active transport of the survival motor neuron protein and the role of exon-7 in cytoplasmic localization. *J. Neurosci.*, **23**, 6627–6637.
 26. Fan, L. and Simard, L.R. (2002) Survival motor neuron (SMN) protein: role in neurite outgrowth and neuromuscular maturation during neuronal differentiation and development. *Hum. Mol. Genet.*, **11**, 1605–1614.
 27. Sharma, A., Lambrechts, A., Hao Le, T., Le, T.T., Sewry, C.A., Ampe, C., Burghes, A.H. and Morris, G.E. (2005) A role for complexes of survival of motor neurons (SMN) protein with gemins and profilin in neurite-like cytoplasmic extensions of cultured nerve cells. *Exp. Cell Res.*, **309**, 185–197.
 28. Setola, V., Terao, M., Locatelli, D., Bassanini, S., Garattini, E. and Battaglia, G. (2007) Axonal-SMN (a-SMN), a protein isoform of the survival motor neuron gene, is specifically involved in axonogenesis. *Proc. Natl Acad. Sci. USA*, **104**, 1959–1964.
 29. Tadesse, H., Deschenes-Furry, J., Boisvenue, S. and Côté, J. (2008) KH-type splicing regulatory protein interacts with survival motor neuron protein and is misregulated in spinal muscular atrophy. *Hum. Mol. Genet.*, **17**, 506–524.
 30. McWhorter, M.L., Monani, U.R., Burghes, A.H. and Beattie, C.E. (2003) Knockdown of the survival motor neuron (Smn) protein in zebrafish causes defects in motor axon outgrowth and pathfinding. *J. Cell Biol.*, **162**, 919–931.
 31. Le, T.T., Pham, L.T., Butchbach, M.E., Zhang, H.L., Monani, U.R., Coovert, D.D., Gavrilina, T.O., Xing, L., Bassell, G.J. and Burghes, A.H. (2005) SMNDelta7, the major product of the centromeric survival motor neuron (SMN2) gene, extends survival in mice with spinal muscular atrophy and associates with full-length SMN. *Hum. Mol. Genet.*, **14**, 845–857.
 32. Kariya, S., Park, G.H., Maeno-Hikichi, Y., Leykehman, O., Lutz, C., Arkovitz, M.S., Landmesser, L.T. and Monani, U.R. (2008) Reduced SMN protein impairs maturation of the neuromuscular junctions in mouse models of spinal muscular atrophy. *Hum. Mol. Genet.*, **17**, 2552–2569.
 33. Kong, L., Wang, X., Choe, D.W., Polley, M., Burnett, B.G., Bosch-Marce, M., Griffin, J.W., Rich, M.M. and Sumner, C.J. (2009) Impaired synaptic vesicle release and immaturity of neuromuscular junctions in spinal muscular atrophy mice. *J. Neurosci.*, **29**, 842–851.
 34. Murray, L.M., Comley, L.H., Thomson, D., Parkinson, N., Talbot, K. and Gillingwater, T.H. (2008) Selective vulnerability of motor neurons and dissociation of pre- and post-synaptic pathology at the neuromuscular junction in mouse models of spinal muscular atrophy. *Hum. Mol. Genet.*, **17**, 949–962.
 35. Biondi, O., Grondard, C., Lécolle, S., Deforges, S., Pariset, C., Lopes, P., Cifuentes-Diaz, C., Li, H., della Gaspera, B., Chanoine, C. et al. (2008) Exercise-induced activation of NMDA receptor promotes motor unit development and survival in a type 2 spinal muscular atrophy model mouse. *J. Neurosci.*, **28**, 953–962.
 36. Murray, L.M., Talbot, K. and Gillingwater, T.H. (2010) Neuromuscular synaptic vulnerability in motor neuron disease: amyotrophic lateral sclerosis and spinal muscular atrophy. *Neuropathol. Appl. Neurobiol.* **36**, 133–156.
 37. Zhang, H., Xing, L., Rossoll, W., Wichterle, H., Singer, R.H. and Bassell, G.J. (2006) Multiprotein complexes of the survival of motor neuron protein SMN with Gemins traffic to neuronal processes and growth cones of motor neurons. *J. Neurosci.*, **26**, 8622–8632.
 38. Todd, A.G., Shaw, D.J., Morse, R., Stebbings, H. and Young, P.J. (2010) SMN and the Gemin proteins form sub-complexes that localise to both stationary and dynamic neurite granules. *Biochem. Biophys. Res. Commun.*, **394**, 211–216.
 39. Glinka, M., Herrmann, T., Funk, N., Havlicek, S., Rossoll, W., Winkler, C. and Sendtner, M. (2010) The heterogeneous nuclear ribonucleoprotein-R is necessary for axonal beta-actin mRNA translocation in spinal motor neurons. *Hum. Mol. Genet.*, **19**, 1951–1966.
 40. Bedford, M.T. and Clarke, S.G. (2009) Protein arginine methylation in mammals: who, what, and why. *Mol. Cell*, **33**, 1–13.
 41. Bachand, F. (2007) Protein arginine methyltransferases: from unicellular eukaryotes to humans. *Eukaryot. Cell*, **6**, 889–898.
 42. Lakowski, T.M. and Frankel, A. (2009) Kinetic analysis of human protein arginine N-methyltransferase 2: formation of monomethyl- and asymmetric dimethyl-arginine residues on histone H4. *Biochem. J.*, **421**, 253–261.
 43. Miranda, T.B., Miranda, M., Frankel, A. and Clarke, S. (2004) PRMT7 is a member of the protein arginine methyltransferase family with a distinct substrate specificity. *J. Biol. Chem.*, **279**, 22902–22907.
 44. Lee, J.H., Cook, J.R., Yang, Z.H., Mirochnitchenko, O., Gunderson, S., Felix, A.M., Herth, N., Hoffmann, R. and Pestka, S. (2005) PRMT7: a new protein arginine methyltransferase that synthesizes symmetric dimethylarginine. *J. Biol. Chem.*, **280**, 3656–3664.
 45. Gonsalvez, G.B., Tian, L., Ospina, J.K., Boisvert, F.M., Lamond, A.I. and Matera, A.G. (2007) Two distinct arginine methyltransferases are required for biogenesis of Sm-class ribonucleoproteins. *J. Cell Biol.*, **178**, 733–740.
 46. Meister, G., Eggert, C., Buhler, D., Brahm, H., Kambach, C. and Fischer, U. (2001) Methylation of Sm proteins by a complex containing PRMT5 and the putative U snRNP assembly factor piCln. *Curr. Biol.*, **11**, 1990–1994.
 47. Friesen, W.J., Massenet, S., Paushkin, S., Wyce, A. and Dreyfuss, G. (2001) SMN, the product of the spinal muscular atrophy gene, binds preferentially to dimethylarginine-containing protein targets. *Mol. Cell*, **7**, 1111–1117.
 48. Friesen, W.J., Paushkin, S., Wyce, A., Massenet, S., Pesiridis, G.S., Van Duyne, G., Rappalber, J., Mann, M. and Dreyfuss, G. (2001) The methylosome, a 20S complex containing JBP1 and piCln, produces

- dimethylarginine-modified Sm proteins. *Mol. Cell. Biol.*, **21**, 8289–8300.
49. Côté, J. and Richard, S. (2005) Tudor domains bind symmetrical dimethylated arginines. *J. Biol. Chem.*, **280**, 28476–28483.
 50. Brahm, H., Meheus, L., de Brabandere, V., Fischer, U. and Luhrmann, R. (2001) Symmetrical dimethylation of arginine residues in spliceosomal Sm protein B/B' and the Sm-like protein LSm4, and their interaction with the SMN protein. *RNA*, **7**, 1531–1542.
 51. Sprangers, R., Groves, M.R., Sinning, I. and Sattler, M. (2003) High-resolution X-ray and NMR structures of the SMN Tudor domain: conformational variation in the binding site for symmetrically dimethylated arginine residues. *J. Mol. Biol.*, **327**, 507–520.
 52. Boisvert, F.M., Côté, J., Boulanger, M.C., Cleroux, P., Bachand, F., Autexier, C. and Richard, S. (2002) Symmetrical dimethylarginine methylation is required for the localization of SMN in Cajal bodies and pre-mRNA splicing. *J. Cell Biol.*, **159**, 957–969.
 53. Hebert, M.D., Shpargel, K.B., Ospina, J.K., Tucker, K.E. and Matera, A.G. (2002) Coilin methylation regulates nuclear body formation. *Dev. Cell*, **3**, 329–337.
 54. Cheng, D., Côté, J., Shaaban, S. and Bedford, M.T. (2007) The arginine methyltransferase CARM1 regulates the coupling of transcription and mRNA processing. *Mol. Cell*, **25**, 71–83.
 55. Cimato, T.R., Ettinger, M.J., Zhou, X. and Aletta, J.M. (1997) Nerve growth factor-specific regulation of protein methylation during neuronal differentiation of PC12 cells. *J. Cell Biol.*, **138**, 1089–1103.
 56. Cimato, T.R., Tang, J., Xu, Y., Guarnaccia, C., Herschman, H.R., Pongor, S. and Aletta, J.M. (2002) Nerve growth factor-mediated increases in protein methylation occur predominantly at type I arginine methylation sites and involve protein arginine methyltransferase 1. *J. Neurosci. Res.*, **67**, 435–442.
 57. Yadav, N., Cheng, D., Richard, S., Morel, M., Iyer, V.R., Aldaz, C.M. and Bedford, M.T. (2008) CARM1 promotes adipocyte differentiation by coactivating PPAR γ . *EMBO Rep.*, **9**, 193–198.
 58. Dacwag, C.S., Bedford, M.T., Sif, S. and Imbalzano, A.N. (2009) Distinct protein arginine methyltransferases promote ATP-dependent chromatin remodeling function at different stages of skeletal muscle differentiation. *Mol. Cell. Biol.*, **29**, 1909–1921.
 59. Chen, S.L., Löffler, K.A., Chen, D., Stallcup, M.R. and Muscat, G.E. (2002) The coactivator-associated arginine methyltransferase is necessary for muscle differentiation: CARM1 coactivates myocyte enhancer factor-2. *J. Biol. Chem.*, **277**, 4324–4333.
 60. Miyata, S., Mori, Y. and Tohyama, M. (2008) PRMT1 and Btg2 regulates neurite outgrowth of Neuro2a cells. *Neurosci. Lett.*, **445**, 162–165.
 61. Fujiwara, T., Mori, Y., Chu, D.L., Koyama, Y., Miyata, S., Tanaka, H., Yachi, K., Kubo, T., Yoshikawa, H. and Tohyama, M. (2006) CARM1 regulates proliferation of PC12 cells by methylating HuD. *Mol. Cell. Biol.*, **26**, 2273–2285.
 62. Hinman, M.N. and Lou, H. (2008) Diverse molecular functions of Hu proteins. *Cell Mol. Life Sci.*, **65**, 3168–3181.
 63. Pascale, A., Amadio, M. and Quattrone, A. (2008) Defining a neuron: neuronal ELAV proteins. *Cell Mol. Life Sci.*, **65**, 128–140.
 64. Deschenes-Furry, J., Perrone-Bizzozero, N. and Jasmin, B.J. (2006) The RNA-binding protein HuD: a regulator of neuronal differentiation, maintenance and plasticity. *BioEssays*, **28**, 822–833.
 65. Mobarak, C.D., Anderson, K.D., Morin, M., Beckel-Mitchener, A., Rogers, S.L., Furneaux, H., King, P. and Perrone-Bizzozero, N.I. (2000) The RNA-binding protein HuD is required for GAP-43 mRNA stability, GAP-43 gene expression, and PKC-dependent neurite outgrowth in PC12 cells. *Mol. Biol. Cell*, **11**, 3191–3203.
 66. Deschenes-Furry, J., Belanger, G., Perrone-Bizzozero, N. and Jasmin, B.J. (2003) Post-transcriptional regulation of acetylcholinesterase mRNAs in nerve growth factor-treated PC12 cells by the RNA-binding protein HuD. *J. Biol. Chem.*, **278**, 5710–5717.
 67. Deschenes-Furry, J., Mousavi, K., Bolognani, F., Neve, R.L., Parks, R.J., Perrone-Bizzozero, N.I. and Jasmin, B.J. (2007) The RNA-binding protein HuD binds acetylcholinesterase mRNA in neurons and regulates its expression after axotomy. *J. Neurosci.*, **27**, 665–675.
 68. Barreau, C., Paillard, L. and Osborne, H.B. (2005) AU-rich elements and associated factors: are there unifying principles? *Nucleic Acids Res.*, **33**, 7138–7150.
 69. Aranda-Abreu, G.E., Behar, L., Chung, S., Furneaux, H. and Ginzburg, I. (1999) Embryonic lethal abnormal vision-like RNA-binding proteins regulate neurite outgrowth and tau expression in PC12 cells. *J. Neurosci.*, **19**, 6907–6917.
 70. Chagnovich, D., Fayos, B.E. and Cohn, S.L. (1996) Differential activity of ELAV-like RNA-binding proteins in human neuroblastoma. *J. Biol. Chem.*, **271**, 33587–33591.
 71. Cuadrado, A., Navarro-Yubero, C., Furneaux, H., Kinter, J., Sonderegger, P. and Munoz, A. (2002) HuD binds to three AU-rich sequences in the 3'-UTR of neuroserpin mRNA and promotes the accumulation of neuroserpin mRNA and protein. *Nucleic Acids Res.*, **30**, 2202–2211.
 72. Joseph, B., Orlian, M. and Furneaux, H. (1998) p21(waf1) mRNA contains a conserved element in its 3'-untranslated region that is bound by the Elav-like mRNA-stabilizing proteins. *J. Biol. Chem.*, **273**, 20511–20516.
 73. Manohar, C.F., Short, M.L., Nguyen, A., Nguyen, N.N., Chagnovich, D., Yang, Q. and Cohn, S.L. (2002) HuD, a neuronal-specific RNA-binding protein, increases the *in vivo* stability of MYCN RNA. *J. Biol. Chem.*, **277**, 1967–1973.
 74. Chung, S., Eckrich, M., Perrone-Bizzozero, N., Kohn, D.T. and Furneaux, H. (1997) The Elav-like proteins bind to a conserved regulatory element in the 3'-untranslated region of GAP-43 mRNA. *J. Biol. Chem.*, **272**, 6593–6598.
 75. Akamatsu, W., Fujihara, H., Mitsuhashi, T., Yano, M., Shibata, S., Hayakawa, Y., Okano, H.J., Sakakibara, S.-I., Takano, H., Takano, T. et al. (2005) The RNA-binding protein HuD regulates neuronal cell identity and maturation. *Proc. Natl Acad. Sci. USA*, **102**, 4625–4630.
 76. Cusco, I., Barcelo, M.J., del Rio, E., Baiget, M. and Tizzano, E.F. (2004) Detection of novel mutations in the SMN Tudor domain in type I SMA patients. *Neurology*, **63**, 146–149.
 77. Sun, Y., Grimmmer, M., Schwarzer, V., Schoenen, F., Fischer, U. and Wirth, B. (2005) Molecular and functional analysis of intragenic SMN1 mutations in patients with spinal muscular atrophy. *Hum. Mutat.*, **25**, 64–71.
 78. Liu, Q. and Dreyfuss, G. (1996) A novel nuclear structure containing the survival of motor neurons protein. *EMBO J.*, **15**, 3555–3565.
 79. Gao, F.B. and Keene, J.D. (1996) Hel-N1/Hel-N2 proteins are bound to poly(A)⁺ mRNA in granular RNP structures and are implicated in neuronal differentiation. *J. Cell Sci.*, **109** (Pt. 3), 579–589.
 80. Perrone-Bizzozero, N. and Bolognani, F. (2002) Role of HuD and other RNA-binding proteins in neural development and plasticity. *J. Neurosci. Res.*, **68**, 121–126.
 81. Bolognani, F., Tanner, D.C., Merhege, M., Deschênes-Furry, J., Jasmin, B. and Perrone-Bizzozero, N.I. (2006) *In vivo* post-transcriptional regulation of GAP-43 mRNA by overexpression of the RNA-binding protein HuD. *J. Neurochem.*, **96**, 790–801.
 82. Kasashima, K., Terashima, K., Yamamoto, K., Sakashita, E. and Sakamoto, H. (1999) Cytoplasmic localization is required for the mammalian ELAV-like protein HuD to induce neuronal differentiation. *Genes Cells*, **4**, 667–683.
 83. Kerppola, T.K. (2006) Design and implementation of bimolecular fluorescence complementation (BiFC) assays for the visualization of protein interactions in living cells. *Nat. Protoc.*, **1**, 1278–1286.
 84. Kerppola, T.K. (2009) Visualization of molecular interactions using bimolecular fluorescence complementation analysis: characteristics of protein fragment complementation. *Chem. Soc. Rev.*, **38**, 2876–2886.
 85. Kasashima, K., Sakashita, E., Saito, K. and Sakamoto, H. (2002) Complex formation of the neuron-specific ELAV-like Hu RNA-binding proteins. *Nucleic Acids Res.*, **30**, 4519–4526.
 86. Lorson, C.L., Strasswimmer, J., Yao, J.M., Baleja, J.D., Hahnen, E., Wirth, B., Le, T., Burghes, A.H. and Androphy, E.J. (1998) SMN oligomerization defect correlates with spinal muscular atrophy severity. *Nat. Genet.*, **19**, 63–66.
 87. Renvoise, B., Khoobarry, K., Gendron, M.C., Cibert, C., Viollet, L. and Lefebvre, S. (2006) Distinct domains of the spinal muscular atrophy protein SMN are required for targeting to Cajal bodies in mammalian cells. *J. Cell Sci.*, **119**, 680–692.
 88. Mohaghegh, P., Rodrigues, N.R., Owen, N., Ponting, C.P., Le, T.T., Burghes, A.H. and Davies, K.E. (1999) Analysis of mutations in the tudor domain of the survival motor neuron protein SMN. *Eur. J. Hum. Genet.*, **7**, 519–525.
 89. Anderson, K.D., Sengupta, J., Morin, M., Neve, R.L., Valenzuela, C.F. and Perrone-Bizzozero, N.I. (2001) Overexpression of HuD accelerates neurite outgrowth and increases GAP-43 mRNA expression in cortical

- neurons and retinoic acid-induced embryonic stem cells *in vitro*. *Exp. Neurol.*, **168**, 250–258.
90. Anderson, K.D., Morin, M.A., Beckel-Mitchener, A., Mobarak, C.D., Neve, R.L., Furneaux, H.M., Burry, R. and Perrone-Bizzozero, N.I. (2000) Overexpression of HuD, but not of its truncated form HuD I + II, promotes GAP-43 gene expression and neurite outgrowth in PC12 cells in the absence of nerve growth factor. *J. Neurochem.*, **75**, 1103–1114.
 91. Li, H., Park, S., Kilburn, B., Jelinek, M.A., Henschen-Edman, A., Aswad, D.W., Stallcup, M.R. and Laird-Offringa, I.A. (2002) Lipopolysaccharide-induced methylation of HuR, an mRNA-stabilizing protein, by CARM1: coactivator-associated arginine methyltransferase. *J. Biol. Chem.*, **277**, 44623–44630.
 92. Mostaqul Huq, M.D., Gupta, P., Tsai, N.P., White, R., Parker, M.G. and Wei, L.N. (2006) Suppression of receptor interacting protein 140 repressive activity by protein arginine methylation. *EMBO J.*, **25**, 5094–5104.
 93. Bowerman, M., Shafey, D. and Kothary, R. (2007) Smn depletion alters profilin II expression and leads to upregulation of the RhoA/ROCK pathway and defects in neuronal integrity. *J. Mol. Neurosci.*, **32**, 120–131.
 94. Shafey, D., MacKenzie, A.E. and Kothary, R. (2008) Neurodevelopmental abnormalities in neurosphere-derived neural stem cells from SMN-depleted mice. *J. Neurosci. Res.*, **86**, 2839–2847.
 95. Anderson, K.D., Merhege, M.A., Morin, M., Bolognani, F. and Perrone-Bizzozero, N.I. (2003) Increased expression and localization of the RNA-binding protein HuD and GAP-43 mRNA to cytoplasmic granules in DRG neurons during nerve regeneration. *Exp. Neurol.*, **183**, 100–108.
 96. Elvira, G., Wasiak, S., Blandford, V., Tong, X.K., Serrano, A., Fan, X., del Rayo Sanchez-Carbente, M., Servant, F., Bell, A.W., Boismenu, D. *et al.* (2006) Characterization of an RNA granule from developing brain. *Mol. Cell. Proteomics*, **5**, 635–651.
 97. Smith, C.L., Afroz, R., Bassell, G.J., Furneaux, H.M., Perrone-Bizzozero, N.I. and Burry, R.W. (2004) GAP-43 mRNA in growth cones is associated with HuD and ribosomes. *J. Neurobiol.*, **61**, 222–235.
 98. Antic, D. and Keene, J.D. (1998) Messenger ribonucleoprotein complexes containing human ELAV proteins: interactions with cytoskeleton and translational apparatus. *J. Cell Sci.*, **111** (Pt. 2), 183–197.
 99. Krichevsky, A.M. and Kosik, K.S. (2001) Neuronal RNA granules: a link between RNA localization and stimulation-dependent translation. *Neuron*, **32**, 683–696.
 100. Tizzano, E.F., Cabot, C. and Baiget, M. (1998) Cell-specific survival motor neuron gene expression during human development of the central nervous system: implications for the pathogenesis of spinal muscular atrophy. *Am. J. Pathol.*, **153**, 355–361.
 101. Zhang, H., Xing, L., Singer, R.H. and Bassell, G.J. (2007) QNQKE targeting motif for the SMN-Gemin multiprotein complex in neurons. *J. Neurosci. Res.*, **85**, 2657–2667.
 102. Gu, W., Pan, F., Zhang, H., Bassell, G.J. and Singer, R.H. (2002) A predominantly nuclear protein affecting cytoplasmic localization of beta-actin mRNA in fibroblasts and neurons. *J. Cell Biol.*, **156**, 41–51.
 103. Briata, P., Forcales, S.V., Ponassi, M., Corte, G., Chen, C.Y., Karin, M., Puri, P.L. and Gherzi, R. (2005) p38-dependent phosphorylation of the mRNA decay-promoting factor KSRP controls the stability of select myogenic transcripts. *Mol. Cell*, **20**, 891–903.
 104. Kiebler, M.A. and Bassell, G.J. (2006) Neuronal RNA granules: movers and makers. *Neuron*, **51**, 685–690.
 105. Rossoll, W. and Bassell, G.J. (2009) Spinal muscular atrophy and a model for survival of motor neuron protein function in axonal ribonucleoprotein complexes. *Results Probl. Cell Differ.*, **48**, 289–326.
 106. Chari, A., Golas, M.M., Klingenhäger, M., Neuenkirchen, N., Sander, B., Englbrecht, C., Sickmann, A., Stark, H. and Fischer, U. (2008) An assembly chaperone collaborates with the SMN complex to generate spliceosomal SnRNPs. *Cell*, **135**, 497–509.
 107. Bertrand, S., Bulet, P., Clermont, O., Huber, C., Fondrat, C., Thierry-Mieg, D., Munnich, A. and Lefebvre, S. (1999) The RNA-binding properties of SMN: deletion analysis of the zebrafish orthologue defines domains conserved in evolution. *Hum. Mol. Genet.*, **8**, 775–782.
 108. Lorson, C.L. and Androphy, E.J. (1998) The domain encoded by exon 2 of the survival motor neuron protein mediates nucleic acid binding. *Hum. Mol. Genet.*, **7**, 1269–1275.
 109. Fukao, A., Sasano, Y., Imataka, H., Inoue, K., Sakamoto, H., Sonenberg, N., Thoma, C. and Fujiwara, T. (2009) The ELAV protein HuD stimulates cap-dependent translation in a Poly(A)- and eIF4A-dependent manner. *Mol. Cell*, **36**, 1007–1017.
 110. Chang, B., Chen, Y., Zhao, Y. and Bruick, R.K. (2007) JMJD6 is a histone arginine demethylase. *Science*, **318**, 444–447.
 111. Webby, C.J., Wolf, A., Gromak, N., Dreger, M., Kramer, H., Kessler, B., Nielsen, M.L., Schmitz, C., Butler, D.S., Yates, J.R. *et al.* (2009) Jmjd6 catalyses lysyl-hydroxylation of U2AF65, a protein associated with RNA splicing. *Science*, **325**, 90–93.
 112. O'Brien, K.B., Alberich-Jordà, M., Yadav, N., Kocher, O., Diruscio, A., Ebralidze, A., Levantini, E., Sng, N.J.L., Bhasin, M., Caron, T. *et al.* (2010) CARM1 is required for proper control of proliferation and differentiation of pulmonary epithelial cells. *Development*, **137**, 2147–2156.
 113. Kim, J., Lee, J., Yadav, N., Wu, Q., Carter, C., Richard, S., Richie, E. and Bedford, M.T. (2004) Loss of CARM1 results in hypomethylation of thymocyte cyclic AMP-regulated phosphoprotein and deregulated early T cell development. *J. Biol. Chem.*, **279**, 25339–25344.
 114. Yadav, N., Lee, J., Kim, J., Shen, J., Hu, M.C., Aldaz, C.M. and Bedford, M.T. (2003) Specific protein methylation defects and gene expression perturbations in coactivator-associated arginine methyltransferase 1-deficient mice. *Proc. Natl Acad. Sci. USA*, **100**, 6464–6468.
 115. Ito, T., Yadav, N., Lee, J., Furumatsu, T., Yamashita, S., Yoshida, K., Taniguchi, N., Hashimoto, M., Tsuchiya, M., Ozaki, T. *et al.* (2009) CARM1/PRMT4 regulates chondrocyte proliferation via arginine methylation of Sox9. *BMC Dev. Biol.*, **9**, 47.
 116. Calvanese, V., Lara, E., Suárez-Alvarez, B., Abu Dawud, R., Vázquez-Chantada, M., Martínez-Chantar, M.L., Embade, N., López-Nieva, P., Horrillo, A., Hmadcha, A. *et al.* (2010) Sirtuin 1 regulation of developmental genes during differentiation of stem cells. *Proc. Natl Acad. Sci. USA*, **107**, 13736–13741.
 117. Wu, Q., Bruce, A., Jedrusik, A., Ellis, P., Andrews, R., Langford, C., Glover, D. and Zernicka-Goetz, M. (2009) CARM1 is required in ES cells to maintain pluripotency and resist differentiation. *Stem Cells*, **27**, 2637–2645.
 118. Fauquier, L., Duboé, C., Joré, C., Trouche, D. and Vandel, L. (2008) Dual role of the arginine methyltransferase CARM1 in the regulation of c-Fos target genes. *FASEB J.*, **22**, 3337–3347.
 119. Ikenaka, K., Miyata, S., Mori, Y., Koyama, Y., Taneda, T., Okuda, H., Kousaka, A. and Tohyama, M. (2006) Immunohistochemical and western analyses of protein arginine N-methyltransferase 3 in the mouse brain. *Neuroscience*, **141**, 1971–1982.
 120. Kousaka, A., Mori, Y., Koyama, Y., Taneda, T., Miyata, S. and Tohyama, M. (2009) The distribution and characterization of endogenous protein arginine N-methyltransferase 8 in mouse CNS. *Neuroscience*, **163**, 1146–1157.
 121. Goulet, I., Gauvin, G., Boisvenue, S. and Côté, J. (2007) Alternative splicing yields protein arginine methyltransferase 1 isoforms with distinct activity, substrate specificity, and subcellular localization. *J. Biol. Chem.*, **282**, 33009–33021.
 122. Bachand, F., Boisvert, F.M., Côté, J., Richard, S. and Autexier, C. (2002) The product of the survival of motor neuron (SMN) gene is a human telomerase-associated protein. *Mol. Biol. Cell*, **13**, 3192–3202.